remote sensing

MDPI

Article

Evaluating Field Sampling Design and LiDAR-Based Approaches for Woody Vegetation Assessment in Reclaimed Wellsite Certification

Angeline Van Dongen, Dmytro Movchan, Charumitha Selvaraj and Dani Degenhardt *

Northern Forestry Centre, Canadian Forest Service, Natural Resources Canada, 5320 122 St NW, Edmonton, AB T6H 2S5, Canada; angeline.vandongen@nrcan-rncan.gc.ca (A.V.D.); dmytro.movchan@nrcan-rncan.gc.ca (D.M.); charumitha.selvaraj@nrcan-rncan.gc.ca (C.S.)
* Correspondence: dani.degenhardt@nrcan-rncan.gc.ca

Highlights

What are the main findings?

- Subjective plot placement overestimated woody stem density compared to random plots at sites with heterogenous vegetation recovery.
- LiDAR data provided valuable spatial information but underestimated woody stem density, particularly at sites with high stem density.

What are the implications of the main findings?

- Random sampling provides a more representative assessment of site conditions, if site-level rather than plot-level criteria are emphasized.
- LiDAR data may be a useful preliminary recovery screening tool or used to inform targeted field sampling.

Abstract

Responsible resource development in Alberta requires the reclamation of disturbed lands to achieve equivalent land capability to pre-disturbance conditions. Vegetation assessments on reclaimed wellsites and oil sand exploration (OSE) sites currently rely on plots placed in areas deemed representative using professional judgement, which may introduce sampling bias. This study compared woody vegetation attributes derived from conventionally placed plots with those from randomly placed plots on certified reclaimed sites. Furthermore, increased sampling intensity was evaluated on a subset of sites. Site-level plot-based estimates were also compared with estimates from uncrewed aerial vehicle light detection and ranging (UAV-LiDAR) and airborne laser scanning (ALS). Woody stem density and height estimates from random and judgment-based plots were generally comparable; however, on sites with spatially heterogeneous recovery, judgment-based placement tended to overestimate woody stem density relative to larger-area sampling. LiDAR data captured spatial patterns of woody vegetation but underestimated stem densities, particularly on high-density, clustered sites.

Keywords: reclamation; wellsite; sampling; assessment; monitoring; LiDAR; UAV-LiDAR; ALS; individual tree detection

Check for updates

Academic Editor: Pinliang Dong

Received: 27 February 2026
Revised: 20 April 2026
Accepted: 30 April 2026
Published: 7 May 2026

Copyright: © 2026 by the authors. Licensee MDPI, Basel, Switzerland. This article is an open access article distributed under the terms and conditions of the Creative Commons Attribution (CC BY) license.

1. Introduction

Responsible natural resource development depends on effective post-disturbance land reclamation to mitigate long-term environmental impacts. In Alberta, there are currently more than 320,000 active, inactive, or decommissioned oil and gas wells across the landscape [1]. These wellsites, along with oil sand exploration (OSE) disturbances, are regulated under the Environmental Protection and Enhancement Act, which requires disturbed land to be reclaimed to a state of equivalent land capability [2]. The 2010 Reclamation Criteria for Wellsites and Associated Facilities for Forested Lands, last updated in 2013, defines the post-reclamation monitoring and assessment framework used to evaluate ecological recovery [3]. Determination of equivalent land capability is based on detailed site assessments (DSA) conducted by a qualified professional, utilizing in situ measurements of landscape, soils, and vegetation attributes relative to adjacent undisturbed reference areas to support reclamation certification. For remote sites that are inaccessible by foot, vehicle, or aerial landing, the assessor may perform an alternative aerial assessment [4].

Vegetation structure, which is intrinsically linked to landscape and soil characteristics, is an important and commonly used indicator of ecosystem recovery in terrestrial ecosystems because the recovery of ecological processes are assumed to follow the establishment of vegetation [5,6]. As such, the assessment of vegetation characteristics on reclaimed sites is a key component of the DSA. Vegetation attributes on reclaimed sites are assessed using a grid-based sampling approach, in which sites are subdivided into grid sections based on the size of the disturbed area [3]. Within each grid section, at a location selected to be representative of the grid section based on professional judgement, a 10 m^2 circular plot (1.78 m radius) is established for vegetation survey. Vegetation success criteria require a minimum of 25% herbaceous canopy cover and 25% woody (trees and shrubs) canopy cover, or a minimum woody stem count of two stems per plot (2000 stems per hectare, sph) for planted sites and five stems per plot (5000 sph) for unplanted sites relying on natural recovery.

The limited number and subjective placement of DSA plots rely heavily on professional judgement, which may introduce unconscious bias. When a sample is not representative, population-level inferences can be misleading [7]. This limitation is particularly evident on sites exhibiting heterogenous or patchy recovery, where judgement-based plot placement may fail to capture local variability in tree regeneration and vegetation cover. Implementing pre-determined stratified random plot locations would reduce subjectivity and improve site representativeness. Additionally, increasing the sampled area, either by increasing the plot number or size, may further enhance the accuracy of the woody species estimates.

Advances in remote sensing technologies offer alternative approaches for assessing forest recovery which add value to site-based assessments with the addition of spatial representation of vegetation [8]. Uncrewed aerial vehicle (UAV)-mounted light detecting and ranging (LiDAR) systems, as well as aircraft-mounted LiDAR (airborne laser scanning, ALS), combined with recent developments in deep learning, enable automated extraction of individual tree attributes across entire sites in substantially less time than conventional ground-based surveys [9,10]. UAV-LiDAR and photogrammetry have been used to evaluate forest recovery on wellsites [9,11]; however, these approaches have not been compared with conventional plot sampling methods. Additionally, a large portion of Alberta's managed forests (93%) have ALS data coverage from forestry-related ALS acquisitions which are increasing at a rate of ~30,000 km^2yr^{-1} [12]. ALS data is operationally used in forest inventories globally on an area basis; however individual tree approaches using these data are prone to detection errors and omissions of small trees, making their applicability to wellsite assessments uncertain [12,13].

In this study, we evaluated recently certified reclaimed wellsites and OSE sites and compared woody species density and height estimates from plots placed using professional judgement with those from randomly placed plots across 14 sites. We further assessed the influence of increasing plot number and plot size on woody species density and height estimates on a subset of six sites. UAV-LiDAR and ALS data were collected from each site to characterize spatial heterogeneity and to compare field-based estimates with LiDAR-derived tree attributes. Specifically, our objectives were to:

1. Compare site-specific woody stem estimates derived from different field sampling methods;
2. Assess whether plot placement method (professional judgment vs. random) significantly influences estimates of woody stem density and/or height;
3. Evaluate whether increasing the number or size of randomly placed plots significantly affects estimates of woody stem density and/or height;
4. Evaluate the performance of UAV-LiDAR and ALS relative to field data in estimating woody species height and density;
5. Use UAV-LiDAR spatial information to investigate sites where randomly placed plots failed to meet reclamation criteria.

2. Materials and Methods

2.1. Study Area

The study area was located near Cold Lake (54°33′0″N, 110°0′3″W) and Conklin (55°37′52″N, 111°4′44″W) in northeastern Alberta (Figure 1). This region was selected due to its high density of recently certified reclaimed wellsites and OSE sites within forested landscapes that coincide with Alberta Biodiversity Monitoring Institute (ABMI)'s aerial LiDAR data coverage. The study area is within Alberta's boreal forest natural region and Central Mixedwood subregion, which is characterized by deciduous stands dominated by mostly aspen (*Populus tremuloides*) or mixed stands of aspen and white spruce (*Picea glauca*), with elevations ranging from ~200 m and 1050 m [14]. Mean daily temperature ranges from −15 °C in January to 18 °C in July while mean monthly precipitation ranges from 13 mm in February to 86 mm in June [15].

2.2. Site Selection

A list of reclamation certificates issued between 2022 and 2025 on public lands or park jurisdictions within the study area was provided by the Alberta Energy Regulator (AER) and used to select candidate study sites. Sites were selected if they were within ABMI's 2022–2023 aerial LiDAR coverage, showed no evidence of post-certification disturbance based on recent high-resolution imagery using Google Earth (accessed April 2025), and were located within 1 km from an access road. DSAs prepared by environmental consultants were obtained through the AER's OneStop Application Query Tool to provide additional site information [17].

Only sites classified as forested and absent of peatlands, transitional areas, or large open water bodies were considered. Wellsites that had been drilled and abandoned were excluded. Sites exhibiting significant third-party disturbances, such as abandoned vehicles, off-road vehicle use, or unmanaged recreational activities, were also excluded due to their potential influence on vegetation recovery. Sites reporting minor variances (e.g., noxious weeds presence or localized soil issues) were retained if the DSA provided justification and confirmed that equivalent land capability criteria was met.

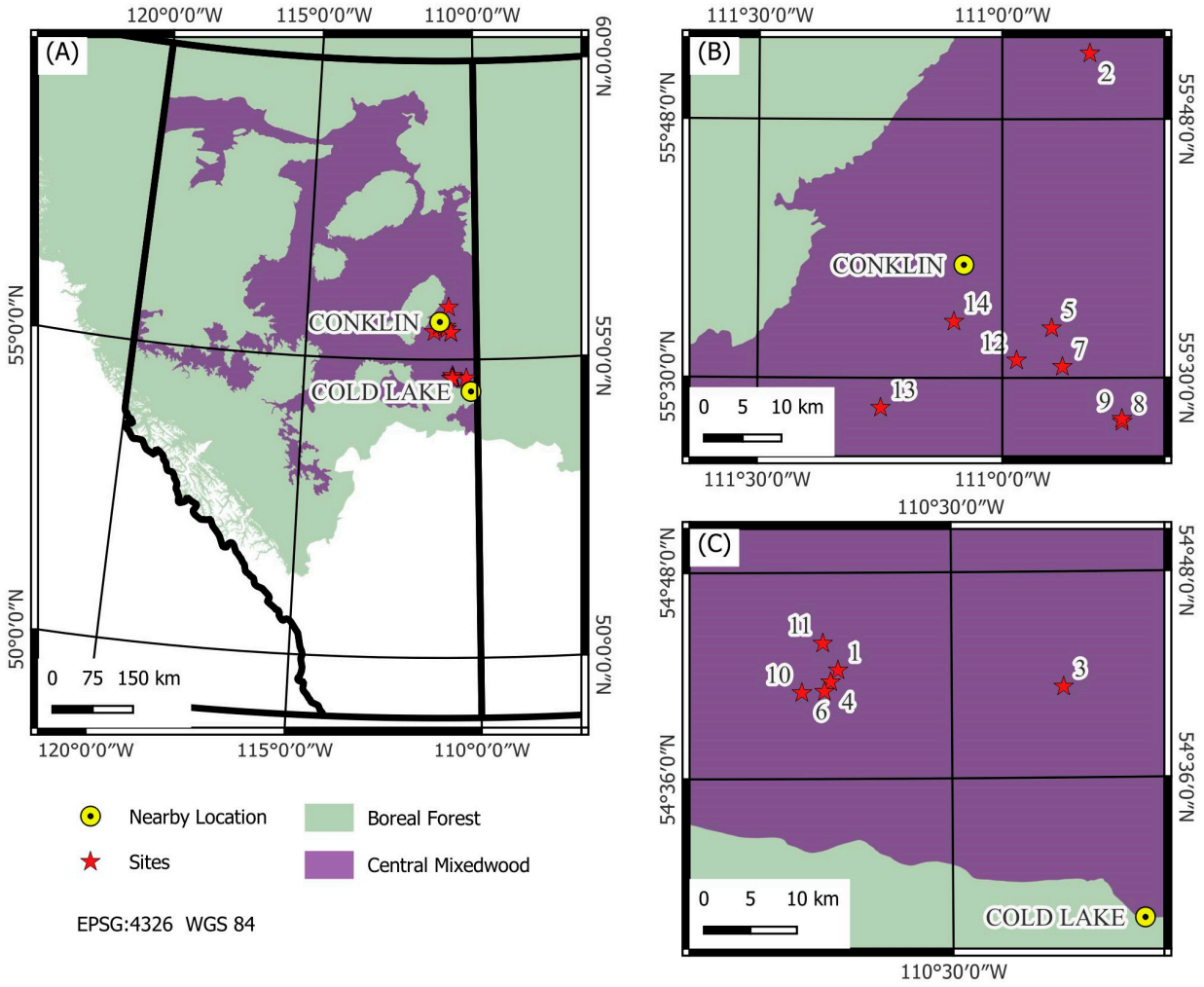


Figure 1. (**A**) Location of the study area within the boreal forest natural region and Central Mixedwood subregion of northeastern Alberta; (**B**) Location of study sites near Conklin, Alberta; (**C**) Location of the study sites near Cold Lake, Alberta. Figure was created using QGIS version 3.32.2 with the boreal forest zone created by Natural Resources Canada [16].

In total, 14 sites were selected, representing both planted and unplanted OSE sites and wellsites spanning a range of disturbance sizes. Sites were abandoned between 2004 and 2018 and certified between 2022 and 2025 (Table A1). Vegetation on the selected sites ranged from early successional assemblages dominated by young, naturally regenerating woody species (~1 m height) to mature stands with dense canopy cover and taller woody vegetation (3–5 m height). Woody vegetation across sites was 58% to 99% deciduous trees and shrubs, primarily balsam poplar (*Populus balsamifera*), willow (*Salix* sp.), red raspberry (*Rubus idaeus*), and prickly wild rose (*Rosa acicularis*) (Table A2). Representative photographs of each site are provided in Figure A1.

2.3. Data Collection

2.3.1. Field Vegetation Sampling

Prior to conducting fieldwork, each site was subdivided into equal-area grid sections in QGIS based on disturbance size, as defined by the lease area in the DSA. Disturbances under 6400 m^2 were divided into four grid sections, while disturbances between 6400 and 14,400 m^2 were divided into nine grid sections [3]. In many cases, the actual disturbed area was smaller than the lease area reported in the DSA; therefore, the footprint of the sites was re-sized to exclude areas with established older trees. Actual disturbed areas are

reported in Table 1. Two random points were generated within each grid section using the Random Points in Polygons tool in QGIS and incorporated into georeferenced maps for field navigation.

Table 1. Lease area (m^2) from the DSA, actual disturbance area (m^2), number of plots, area sampled (m^2), and site area covered (%) for each plot type on each site. Plot types include 10 m^2 professional judgement (PJ) and 10 m^2 random (R) plots at all sites, while sites selected for increased sampling also include an additional 10 m^2 random (R+) plot and a large 50 m^2 random (RL) plot.

Site ID	Lease Area (m^2)	Actual Disturbed Area (m^2)	Number of Plots				Area Sampled (m^2)				Site Area Covered (%)			
			PJ	R	R+	RL	PJ	R	R+	RL	PJ	R	R+	RL
1	8100	6558	9	9			90	90			1.4	1.4		
2	8100	4907	9	9	18	9	90	90	180	450	1.8	1.8	3.7	9.2
3	8000	4808	9	9	18	9	90	90	180	450	1.9	1.9	3.7	9.4
4	8250	7833	9	9	18	9	90	90	180	450	1.1	1.1	2.3	5.7
5	4770	4502	4	4	8	4	40	40	80	200	0.9	0.9	1.8	4.4
6	5400	4521	4	4	-	-	40	40	-	-	0.9	0.9	-	-
7	5400	4832	4	4	8	4	40	40	80	200	0.8	0.8	1.7	4.1
8	5400	4734	4	4	-	-	40	40	-	-	0.8	0.8	-	-
9	5400	3609	4	4	-	-	40	40	-	-	1.1	1.1	-	-
10	5400	4454	4	4	-	-	40	40	-	-	0.9	0.9	-	-
11	5400	4444	4	4	-	-	40	40	-	-	0.9	0.9	-	-
12	5400	4883	4	4	-	-	40	40	-	-	0.8	0.8	-	-
13	5400	4832	4	4	8	4	40	40	80	200	0.8	0.8	1.7	4.1
14	5400	4968	4	4	-	-	40	40	-	-	0.8	0.8	-	-

Field data collections were conducted between May and August 2025. At each of the 14 certified reclaimed sites, woody vegetation was surveyed using two plot placement approaches within each stratified grid sections: professional judgement and random sampling (Table 1). For the professional judgement approach, one 1.78 m radius (10 m^2) circular plot was established per grid section at a location deemed representative, as per the Reclamation Criteria [3]. For the random sampling method, one 1.78 m radius circular plot was placed at a pre-determined random location within each grid section.

A subset of six sites was selected for increased sampling intensity (Table 1). To limit field time, increased sampling was conducted on sites that exhibited low or heterogenous woody density upon initial site assessment. Increased sampling included an additional randomly located 1.78 m radius plot and a larger 3.99 m radius (50 m^2) circular plot in each grid section. The larger plot shared the same center point as the additional random plot. The lease area, actual disturbed area, number of plots, total area sampled, and percentage of site area surveyed for each plot type at each site are summarized in Table 1.

In all plots, center-point coordinates were recorded using an Emlid Reach RS2+ GNSS (Esztergom, Hungary) unit and corrected using post-processing kinematics. Woody, non-trailing vegetation was surveyed by recording the species and measuring the height of all individuals taller than 1.3 m. Woody individuals shorter than 1.3 m were counted and an average height was recorded for each species. To avoid double-counting in the larger plots, which shared the center point of the additional random plot, woody vegetation located near the edge of the 10 m^2 plot was marked with tree paint prior to expanding sampling to the 50 m^2 plot. Vegetation was then recorded between the 1.78 m and 3.99 m marked radius boundaries. Data from the smaller plot were subsequently incorporated into the larger plot dataset.

To validate the UAV-LiDAR detection and height accuracy, 602 randomly selected reference trees including white spruce, lodgepole pine, tamarack, willow, balsam poplar, paper birch, and aspen across six sites were geolocated using an Emlid Reach RS2+ GNSS unit and their heights were measured using either a measuring tape or height pole.

2.3.2. LiDAR Data Acquisition and Processing

UAV-LiDAR data were collected at each site using a DJI Matrice 300 RTK drone equipped with a DJI Zenmuse L2 sensor (DJI Technology Co., Ltd., Shenzhen, China). Flights were conducted at an altitude of 50 m and a speed of 5 m s^{-1}, with 70% side and forward overlap. The LiDAR sensor operated in penta-return mode at a sampling rate of 240 Hz with repetitive scanning and RGB acquisition. Resulting point cloud density was 1734 points m^{-2}. An Emlid Reach RS2+ GNSS base station collected positional data for a minimum of two hours per site to improve spatial accuracy and was corrected using precise point processing. UAV-LiDAR data were processed using DJI Terra Pro software (v. 5.1.0) and exported as .laz point cloud files.

ALS data were obtained from ABMI acquired during campaigns near Conklin and Cold Lake. The ALS point density was either 12, 24, or 29 points m^{-2}, depending on the acquisition (Table A3). UAV and aerial LiDAR point clouds were clipped to the actual disturbance area. In cases where mature trees occurred along edges of the site, these trees were manually removed from the point cloud in CloudCompare to prevent inclusion of adjacent forest vegetation.

Individual tree locations and heights were extracted from the UAV-LiDAR and ALS point clouds using the TreeAIBox plugin in CloudCompare [10] (Figure 2). TreeAIBox models were trained on very high-density point clouds (>1000 points m^{-2}) and worked well on UAV-LiDAR data using default settings; however, due to the lower point density (<50 points m^{-2}) of the ALS data, optimization of voxel resolution parameters was required to reduce under-detection of canopy structures and enhance segmentation accuracy. Following evaluation across ALS datasets, a horizontal (XY) resolution of 0.2 m and vertical (Z) resolution of 0.8 m were selected as optimal. This parameter combination produced the highest mean detection rate exceeding alternative configurations by 5–20% on average (Figure A2). While site-specific variability was observed, this configuration provided robust overall performance by prioritizing detection in low-density point cloud environments.

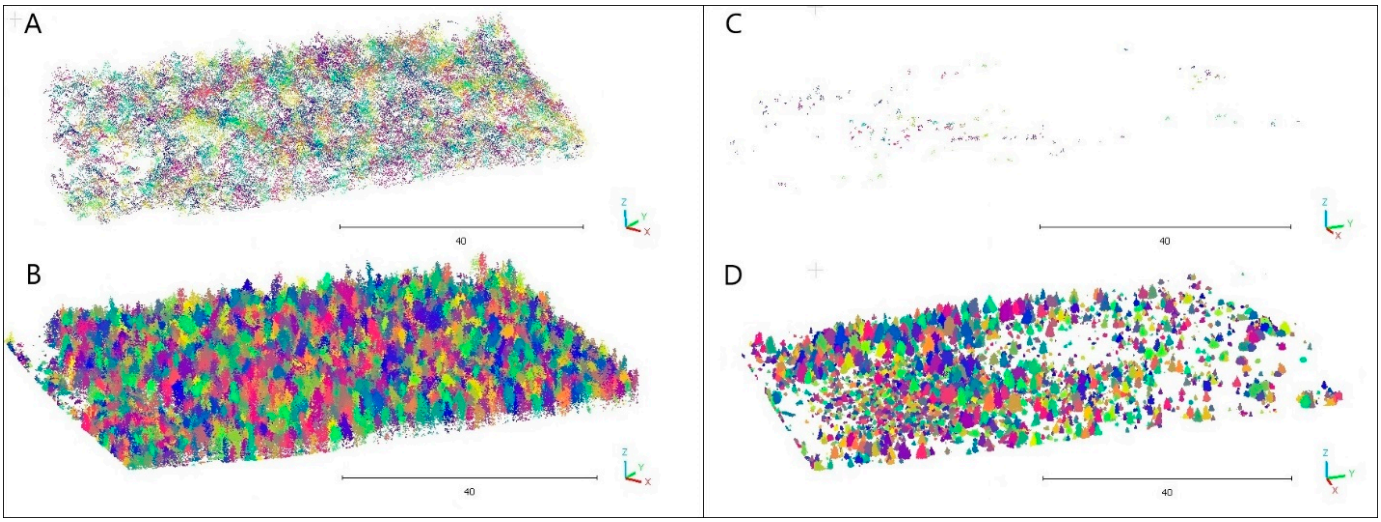


Figure 2. Individual trees segmented from (**A**) Site 8 ALS data; (**B**) Site 8 UAV-LiDAR data; (**C**) Site 14 ALS data; (**D**) Site 14 UAV-LiDAR (**D**). Unique random colours indicate individual trees.

Site-level individual tree analysis was restricted to woody stems taller than 1.3 m due to reduced detection of shorter vegetation. The threshold of 1.3 m was chosen because it is often used to distinguish trees from seedlings and should represent vegetation that is LiDAR-detectable since detection rates generally drop for trees below 1 m [9,18] For each site, woody stem density was calculated by dividing the number of detected stems taller

than 1.3 m by the disturbance area (hectares). The mean height with standard deviation (SD) for all stems taller than 1.3 m was also calculated for each site.

2.4. Data Analysis

Data analysis and visualizations were conducted in R statistical software (v. 4.5.1) [19]. Woody vegetation was grouped into two analytical categories: all woody species, and a subset including only individuals taller than 1.3 m. Although the wellsite reclamation criteria do not impose a height threshold, this subset was included to better represent tree structure by excluding low shrubs and to improve comparability with LiDAR-derived estimates, which were restricted to trees taller than 1.3 m. The response variables were woody stem density and height, which were compared across four plot types: professional judgement, random, increased random, and large random. Data were summarized at plot level, with heights averaged per plot and stem counts converted to density (sph) to allow comparison across plot sizes and reclamation criteria. Descriptive statistics (mean and SD) were used to visualize differences among sampling methodologies within individual sites prior to inferential analysis.

Two sets of analyses were conducted: one comparing professional judgement and random plot types across all 14 sites, and another comparing all four plot types across the six sites with increased sampling intensity. The increased random category includes both the original random plot and the additional random plot within each grid section, resulting in a doubled sample size for this category; however, half of the observations were shared with the single random plot dataset. Similarly, the large plot category includes data from the additional random plot, as both plot types shared the same plot center.

To evaluate the effect of plot type on woody stem density and height estimates, generalized linear mixed models were fitted using the *glmmTMB* package. Plot type was treated as a fixed effect, with site included as a random effect to account for the non-independence of plots within sites. Density data were modeled using either a gamma or Tweedie (when zero values were present) distribution, with a log link, while height data were modeled using a gamma distribution with log link. Model diagnostics were assessed using the *DHARMa* package, and a dispersion formula was applied where necessary to address abnormal residual patterns. Wald χ^2 tests were conducted using the *Anova0* function from the *car* package to assess the significance of the plot type effect ($\alpha = 0.05$). Estimated marginal means were calculated using the *emmeans* package, with Tukey-adjusted *p*-values applied to multiple comparisons. Model specifications and ANOVA results based on Wald χ^2 test results are provided in Table A4, and model diagnostic outputs are presented in Figures A6–A13.

3. Results

3.1. Site-Specific Comparisons Between Field Sampling Approaches

Mean woody stem density across all plot types and sites ranged from 7644 sph (Site 2) to 85,250 sph (Site 12), exceeding the minimum reclamation density criteria (Figure 3). High stem densities were frequently associated with shrub-dominated communities, particularly willow, red raspberry, and prickly wild rose. Stem density of woody species taller than 1.3 m ranged from 250 sph (Site 5) to 37,750 sph (Site 9) (Figure 4).

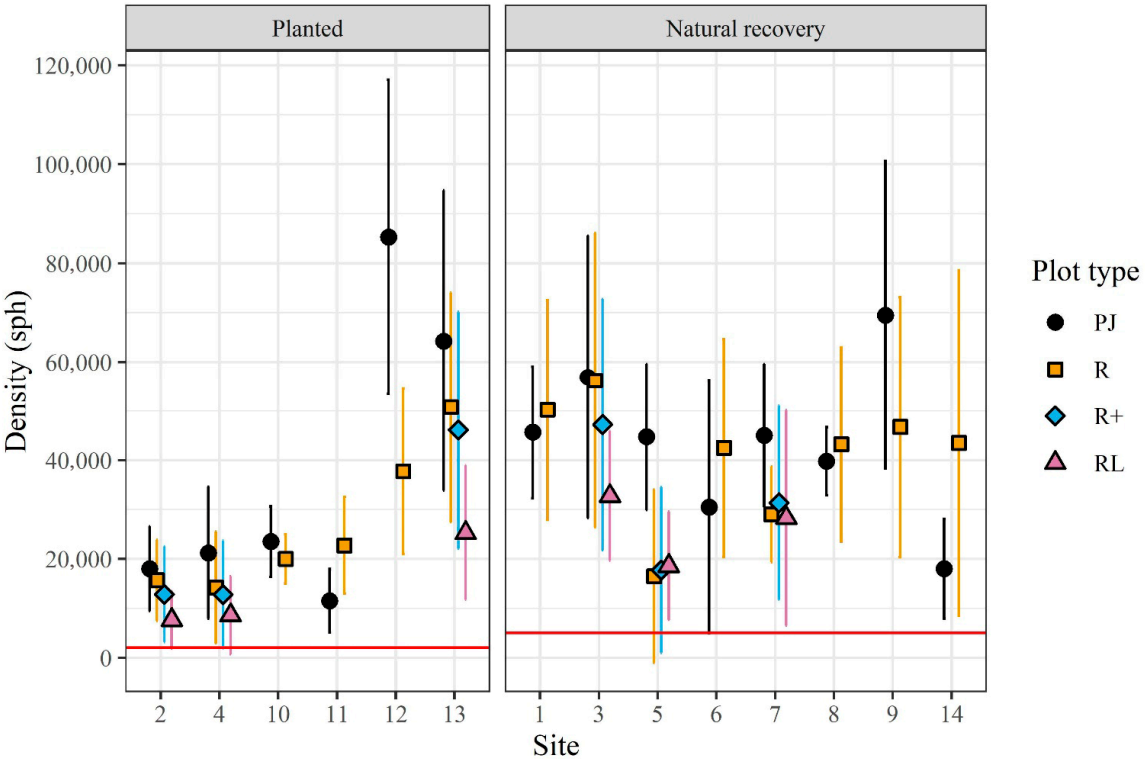


Figure 3. Woody species mean density from each plot type: Professional judgement (PJ, black), random (R, orange), additional random (R+, blue), and large random (RL, pink) by site, grouped by revegetation method. Error bars indicate one SD from the mean. Red horizontal line indicates the minimum required plot density by revegetation method.

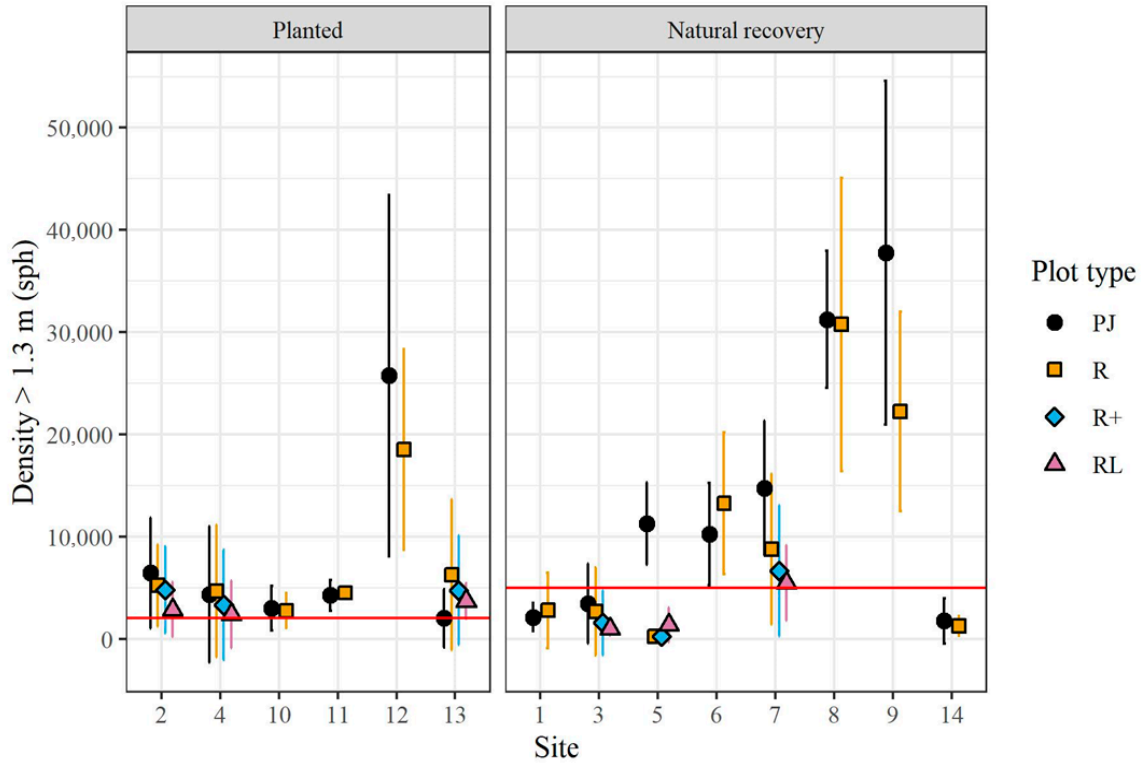


Figure 4. Woody species taller than 1.3 m mean density from each plot type: Professional judgement (PJ, black), random (R, orange), additional random (R+, blue), and large random (RL, pink) by site, grouped by revegetation method. Error bars indicate one SD from the mean. Red horizontal line indicates the minimum required plot density depending on revegetation method.

Across individual sites, density estimates derived from different plot types were generally comparable, as indicated by the overlap in their means ± SDs (Figures 3 and 4). However, some sites had larger differences in mean estimates between plot types. Specifically, Sites 5 and 12 yielded higher mean woody stem densities from professional judgment plots relative to the other plot types (Figure 3), with differences at Site 5 more pronounced for woody species taller than 1.3 m (Figure 4).

Mean height estimates across plot types within individual sites were generally comparable, as indicated by the overlapping mean ± SD ranges (Figure 5). Nonetheless, professional judgement plots yielded higher mean heights at Sites 5, 6, and 11, while random plots captured higher mean heights at Site 12. When analyses were restricted to woody species taller than 1.3 m, differences among plot types were more evident at Sites 5 and 14 (Figure 6).

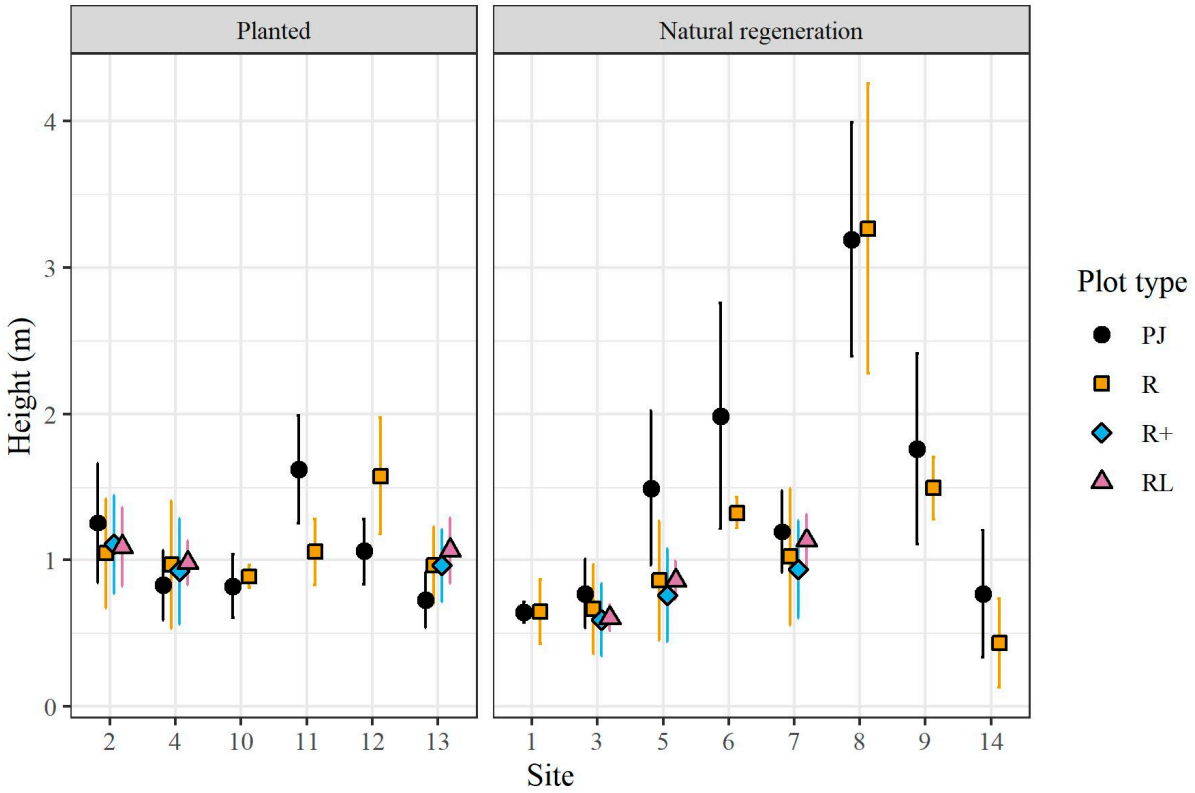


Figure 5. Woody species mean height from each plot type: Professional judgement (PJ, black), random (R, orange), additional random (R+, blue), and large random (RL, pink) by site, grouped by revegetation method. Error bars indicate one SD from the mean.

3.2. Effect of Sampling Methods on Height and Density Estiamtes

Across all 14 sites, no significant differences were detected between professional judgement and random plot types for mean woody stem density, mean woody species height, mean woody stem density of species taller than 1.3 m, or mean height of woody species taller than 1.3 m (Table 2).

Statistical models comparing woody species metrics across the six sites with increased sampling intensity detected a significant effect of plot type on total stem density, with professional judgment, random, and additional random plots yielding significantly higher density estimates than larger random plots (Table 3). For woody species taller than 1.3 m, professional judgment plots produced significantly higher density estimates than both the additional random and larger random plots (Table 3).

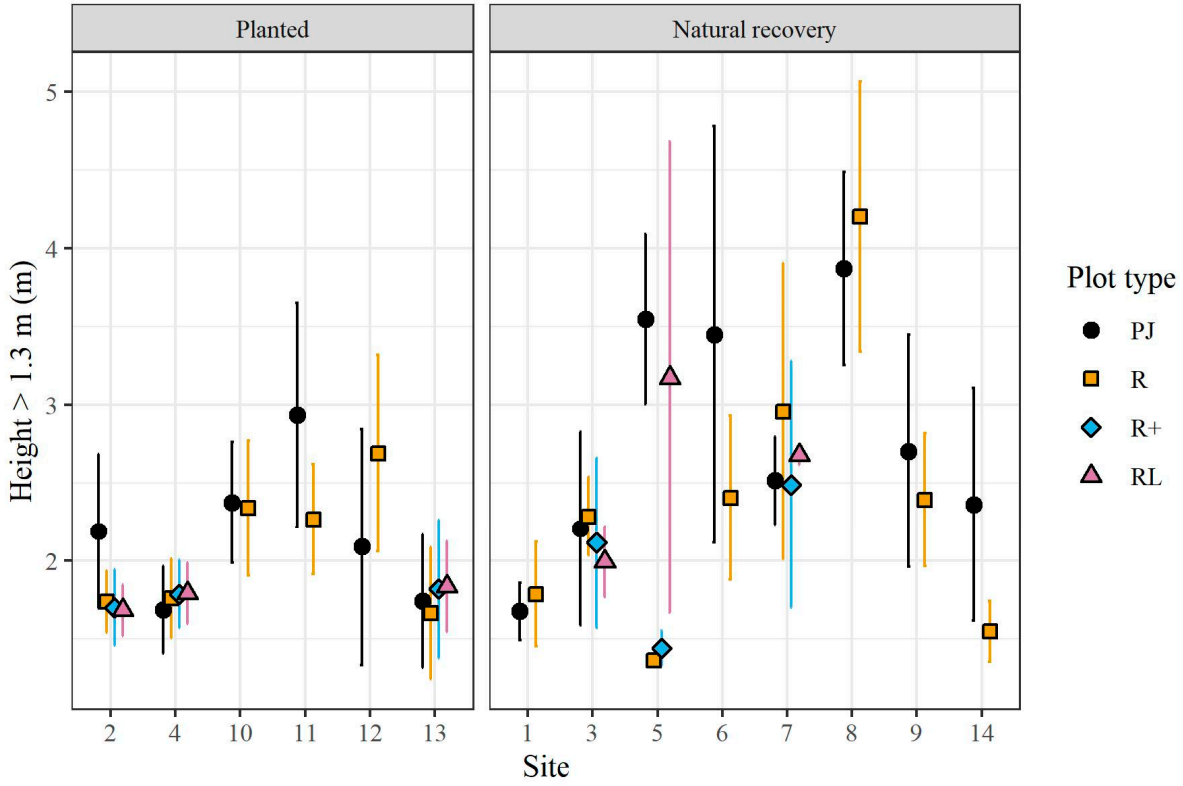


Figure 6. Woody species taller than 1.3 m mean height from each plot type: Professional judgement (PJ, black), random (R, orange), additional random (R+, blue), and large random (RL, pink) by site, grouped by revegetation method. Error bars indicate one SD from the mean.

Table 2. Mean and standard error (SE) of density (sph) and height (m) of all woody species and woody species taller than 1.3 m from professional judgement (PJ) plots and random (R) plots across 14 sites with letters indicating significant differences and probabilities (*p*-value).

Group	Variable	Plot Type		*p* Value
		PJ	R	
All woody species	Density (sph)	36, 858 (4814) [a]	32,676 (4290) [a]	0.17
	Height (m)	1.16 (0.14) [a]	1.06 (0.12) [a]	0.11
Woody species taller than 1.3 m	Density (sph)	6874 (1759) [a]	6374 (1636) [a]	0.49
	Height (m)	2.35 (0.17) [a]	2.25 (0.16) [a]	0.33

Table 3. Mean and standard error (SE) of density (sph) and height (m) of all woody species and woody species taller than 1.3 m from professional judgement (PJ) plost, random (R) plots, additional random (R+) plots, and larger random (RL) plots across six sites with letters indicating significant differences and probabilities (*p*-value).

Group	Variable	Plot Type				*p* Value
		PJ	R	R+	RL	
All woody species	Density (sph)	36,236 (8284) [c]	27,580 (6387) [bc]	24,670 (5475) [b]	17,394 (4116) [a]	<0.001
	Height (m)	1.01 (0.09) [a]	0.92 (0.08) [a]	0.88 (0.07) [a]	0.93 (0.08) [a]	0.23
Woody species taller than 1.3 m	Density (sph)	6120 (1434) [b]	4379 (1168) [ab]	3324 (768) [a]	2434 (554) [a]	<0.001
	Height (m)	2.11 (0.16) [a]	2.01 (0.15) [a]	1.95 (0.14) [a]	1.95 (0.14) [a]	0.33

3.3. LiDAR Results

3.3.1. Reference Tree Results

The geolocated reference trees were 25% coniferous and 75% deciduous or shrub with a mean field-measured height of 2.88 m. The overall UAV-LiDAR detection rate for the reference trees was 50%, with a mean height of 3.04 m. Detection rates varied by species with the willow and paper birch having the lowest detection rate (44%) and spruce having the highest detection rate (62%). Of the non-detected reference trees, 7% were in open areas, but were indistinguishable from the ground layer (mean height 0.9 m); however, the mean height of undistinguished deciduous and shrub species was higher (1.16 m) compared to coniferous species (0.53 m). The remaining 43% of undetected reference trees were not correctly segmented (mean height of 3.02 m) due to interference from adjacent trees in areas with overlapping crowns or canopies.

Height accuracy was evaluated for 174 reference trees which could be identified and matched in the point cloud with high certainty. The mean height of these trees was 3.56 m. Comparison between UAV-LiDAR-derived and field-measured heights showed strong agreement, with a coefficient of determination (R^2) of 0.98 and root mean square error (RMSE) of 23 cm (6.5%), with UAV-LiDAR showing a slight tendency to underestimate tree heights relative to field measurements.

Due to the lower spatial resolution of the ALS data and high stem densities, individual reference trees could not be confidently distinguished and matched within the point cloud for ALS validation.

3.3.2. Site-Level Comparisons Between LiDAR and Field Data

UAV-LiDAR and ALS data were compared with plot-based field data to evaluate the accuracy of LiDAR surveys in representing site-level vegetation attributes. All plots within each site were included to maximize the proportion of site area sampled (Table 2). Because LiDAR individual tree detection is known to be poor for small trees [9,18], the comparison between plot data and LiDAR data was restricted to woody species taller than 1.3 m.

Both UAV-LiDAR and ALS-derived height estimates aligned well with the plot-based estimates when mean and SD were considered; however, the LiDAR-based estimates exhibited a slight tendency to overestimate mean site height (Table 4).

Table 4. Mean and SD of height and density results for woody stems taller than 1.3 m from all field plots, UAV-LiDAR, and ALS at each site. The percentage of plot-based mean site density captured by the UAV-LiDAR and ALS data is also shown for each site.

Site	# Field Plots (n)	Height (m)			Density (sph)			% Plot Density Captured	
		Field Plots	UAV-LiDAR	ALS	Field Plots	UAV-LiDAR **	ALS **	UAV-LiDAR	ALS
1 *	18	1.7 (0.2)	2.0 (0.7)	2.1 (0.5)	2444 (2727)	1758	300	72	12
2	27	1.9 (0.4)	2.2 (1.0)	2.4 (0.9)	4837 (4318)	2480	626	51	13
3 *	27	2.1 (0.4)	3.4 (1.9)	4.6 (2.5)	2356 (3400)	1462	262	62	11
4	27	1.7 (0.2)	2.0 (0.6)	2.2 (0.9)	3800 (5568)	2992	111	79	3
5 *	12	3.1 (1.1)	4.0 (2.2)	3.9 (1.6)	4283 (5654)	1628	829	38	19
6 *	8	2.9 (1.1)	3.9 (1.6)	3.5 (1.2)	11,750 (5825)	4340	2488	37	21
7 *	12	2.7 (0.5)	3.4 (1.7)	3.4 (1.4)	9650 (6822)	2303	687	24	7
8 *	8	4.0 (0.7)	5.4 (1.6)	3.8 (1.2)	31,000 (10,379)	4193	2936	14	9
9 *	8	2.5 (0.6)	4.3 (1.7)	3.6 (1.3)	30,000 (15,185)	4752	2674	16	9
10	8	2.4 (0.4)	2.7 (0.8)	2.2 (0.4)	2875 (1808)	2178	361	76	13
11	8	2.6 (0.6)	2.7 (1.0)	2.7 (0.9)	4375 (1061)	2306	317	53	7
12	8	2.4 (0.7)	3.0 (1.2)	2.3 (0.6)	22,125 (13,799)	5089	1855	23	8
13	12	1.7 (0.3)	2.2 (0.5)	1.6 (0.2)	3983 (4599)	2786	91	70	2
14 *	8	2.0 (0.7)	1.9 (0.5)	1.6 (0.3)	1500 (1604)	1027	10	68	1

* = Unplanted sites relying on natural recovery. ** = Density based on the total number of detected stems; no SD.

In contrast, density estimates were strongly influenced by site conditions, including stem density, height, and species composition. Across sites, LiDAR detection rate (expressed as the percentage of plot-based stem density captured) was between 14% and 79% for UAV-LiDAR, while ALS consistently detected fewer stems, capturing between 1% and 21% of the plot-based mean density (Table 4). When plot-based densities were below 4000 sph, UAV-LiDAR and ALS density estimates generally fell within the range of mean ± SD of plot-based values, except for Site 10, where the ALS estimate was below the plot mean (Table 2). At sites with higher plot-based stem densities (>10,000 sph; Sites 6,7,8,9, and 12), both UAV-LiDAR and ALS substantially underestimated woody stem density. UAV-LiDAR captured between 14% and 37% of plot-based density at these sites, while ALS captured between 7% and 21%. Even under these high-density conditions, the maximum density detected was 5089 sph for UAV-LiDAR and 2936 sph for ALS (Table 4).

Using all 14 sites, correlations were examined between LiDAR detection rate and field-based mean height and stem density. For UAV-LiDAR, detection rate exhibited a strong and statistically significant negative relationship with plot-based stem density (Pearson $r = -0.841$, $p = 0.0002$; Spearman $\rho = -0.859$, $p = 0.0001$), indicating a marked decline in detection performance as stem density increased. UAV-LiDAR detection rate was also strongly negatively correlated with mean plot-based height (Pearson $r = -0.738$, $p = 0.0026$; Spearman $\rho = -0.740$, $p = 0.0025$). Although this suggests reduced detection in taller stands, sites with greater mean height in this dataset were also characterized by higher stem densities, indicating that the apparent height effect is likely confounded by density.

In contrast, ALS detection rate showed no meaningful relationship with plot-based stem density (Pearson $r = 0.035$, $p = 0.9066$; Spearman $\rho = 0.170$; $p = 0.5617$), suggesting that ALS detection was largely insensitive to variation in stem density across sites. ALS detection rate exhibited a moderate positive association with mean height (Pearson $r = 0.400$, $p = 0.1566$; Spearman $\rho = 0.367$, $p = 0.1968$), indicating a tendency toward improved detection in taller stands; however, this relationship was not statistically significant.

3.4. Explaining Plot-Level Density Failures

Of the 14 study sites, three sites (21%), Sites 2, 4 and 5, failed to meet plot-level minimum density criteria (2000 sph for planted sites; 5000 sph for natural recovery sites) in at least one randomly placed plot. For these three sites, the UAV-LiDAR data were used to evaluate vegetation recovery patterns across the entire site, providing insights into why some random plots failed to meet reclamation criteria and to assess overall site-level recovery. UAV-LiDAR-derived stem distributions revealed highly heterogeneous spatial patterns at these sites (Figures A3–A5).

At Site 2, a planted wellsite, two additional random plots and one large random plot did not meet the minimum density threshold of 2000 sph (equivalent to two stems in a 10 m^2 plot or ten stems in a 50 m^2 plot) (Figure A3). Despite these failed plots, overall site-level woody stem density was high, ranging from 7644 ± 5803 to 18,000 ± 8588 sph depending on plot type. UAV-LiDAR-derived density for Site 2 was 2480 sph (stems > 1.3 m), meeting minimum stem density criteria, although areas of lower stem density were evident near the center of the wellsite where the wellhead was placed (Figure A3).

At Site 4, another planted wellsite, two random plots, two additional random plots, and two large random plots failed to meet minimum density criteria (Figure A4). Nonetheless, site-level woody stem density remained high, ranging from 8600 ± 7890 to 21,222 ± 13,348 sph across plot types. UAV-LiDAR-derived density was 2992 sph (stems > 1.3 m), with stems primarily concentrated on one half of the site (Figure A4).

At Site 5, a natural recovery wellsite, one random plot and one additional random plot failed to meet the minimum density threshold of 5000 sph (Figure A5). Site-level woody

stem density ranged from 16,500 ± 17,521 to 44,750 ± 14,886 sph; however, densities of woody species taller than 1.3 m were substantially lower, ranging from 250 ± 463 to 11,250 ± 4031 sph depending on plot type. UAV-LiDAR-derived density for Site 5 was 1628 sph (stems > 1.3 m), indicating that a large proportion of woody stems consisted of small saplings or shrubs under 1.3 m (Figure A5). Spatial information provided by the UAV-LiDAR data also indicated linear features consistent with trail networks, which were not documented in the corresponding DSA.

4. Discussion

4.1. Field Sampling Methods

Random sampling enables population-level inferences by ensuring that every sampling unit has an equal probability of selection, thereby creating the inferential link between sampled and unsampled units [7]. On this basis, we hypothesized that plots placed using professional judgement would yield biased estimates of woody vegetation attributes. However, across all 14 study sites, no significant differences were detected between professional judgement and randomly placed plots for woody stem density or height. Based on our limited number of sites sampled, this result indicates that, on the site scale and for the plot sizes evaluated, professional judgement plots produced estimates comparable to those obtained through random sampling, suggesting that either approach may be suitable for reclamation certification assessments. Stratification of site into grid sections likely aided the performance of both approaches by capturing variability among strata, consistent with established sampling theory [7].

While all the professional judgement plots exceeded the minimum stem density criteria, some randomly placed plots failed to meet plot-level minimum density criteria, even when site-level averages exceeded regulatory thresholds. This finding highlights a limitation of applying rigid plot-level criteria in reclamation certification, suggesting that site-level averages may provide a more appropriate basis for evaluating performance when random sampling is employed. Allowing a limited number of plot-level failures may be necessary to maintain statistical rigor while avoiding failing sites that meet overall reclamation objectives.

At the subset of six sites subjected to increased sampling intensity, plot type significantly influenced density estimates. Professional judgement plots yielded density estimates similar to single random plots but consistently higher than estimates derived from increased numbers or larger random plots. This pattern likely reflects two interacting factors: first, larger sampling areas capture a greater proportion of the site area and therefore provide more representative estimates; and second, professional judgment plots may preferentially target areas with higher woody stem densities. Samples that are biased or not representative can result in misleading population-level inferences [7]. Notably, the six sites selected for increased sampling were initially chosen because of perceived heterogeneity or low stem densities, conditions under which sampling strategy has been shown to strongly influence outcomes [20]. These results suggest that plot placement effects are amplified on sites with more heterogenous or uneven recovery. In spatially autocorrelated or patchy environments, multi-scale sampling approaches that include sub-plots may better capture variability than single-scale designs [21].

Unexpectedly, total stem densities from larger random plots were significantly lower than those from an increased number of smaller random plots. This discrepancy may reflect observer error associated with counting woody stems, especially small stems over larger plot areas. The absence of significant differences among plot types for densities of woody species taller than 1.3 m supports this interpretation, indicating that smaller stems were more likely to be undercounted, especially in larger plots. Accordingly, we do not

recommend using 50 m^2 plots for assessing small woody stems on reclaimed OSE sites or wellsites.

Mean woody species height was not significantly influenced by plot type, suggesting that height is more spatially uniform across sites, and less sensitive to plot placement and size than stem density.

Overall, although mean density derived from random and professional judgement plots were statistically similar, random plot estimates aligned more closely with increased sampling approaches, particularly on sites with heterogeneous recovery where professional judgement plots overestimated density. Together these results indicate that randomly placed plots may provide more representative estimates of vegetation attributes on sites with spatially heterogenous recovery. Therefore, we recommend the use of pre-determined random plot locations for field-based reclamation assessment, with the caveat that site-level density should take precedent over strict plot-level thresholds.

4.2. LiDAR Assessments

Comparisons between plot-based measurements and LiDAR-derived estimates provide insight into the strengths and limitations of LiDAR in vegetation assessments for certification purposes. Total woody stem densities derived from both UAV-LiDAR and ALS data were consistently lower than plot-based estimates. The accuracy of individual tree detection from LiDAR is influenced by both forest conditions and individual tree detection algorithms; however, forest structure, particularly stem density and spatial clustering, has been shown to have a greater effect on detection performance than algorithm choice alone [22]. At the OSE sites and wellsites examined here, underestimation of woody stem density from LiDAR data was primarily attributable to under-detection of low-stature vegetation and poor tree segmentation in areas of high stem density.

The omission of low vegetation, including shrubs and juvenile trees, is a well-documented limitation of LiDAR, particularly in complex, mixed species and multilayered forest environments [12,23]. The mean height of undetected reference trees from UAV-LiDAR surveys was 0.9 m, consistent with previous studies reporting reduced detection rates for trees shorter than 1 m [9,18,24]. This limitation reflects both point cloud resolution constraints and the design of the TreeAIBox models, which were trained primarily on tree structures rather than low shrubs [10]. In addition, detection rates of small trees are sensitive to the method used to derive the terrain model for separating vegetation from the ground [10,24]. For these reasons, comparisons between field and LiDAR data were restricted to trees taller than 1.3 m, consistent with previous LiDAR-based individual tree detection studies that applied similar height thresholds [11,25,26]; however, the low detection rate of low-stature vegetation is an important limitation for the application of LiDAR in reclamation certification.

UAV-LiDAR detected 50% of the randomly selected reference trees, which is lower than the detection performance reported by Movchan et al. [9], who also used TreeAIBox with UAV-LiDAR data on reclaimed wellsites and achieved reference tree detection rates over 90%; however, their trees were above 1.5 m and sites were lower density, generally below 2000 sph. Most other studies report tree detection accuracies based on stem mapped plot data (Table 5); therefore, it should be noted that our detection rate pertains to a subset of individual reference trees when making comparisons. Furthermore, this study is unique in its comparison of wall-to-wall LiDAR data with plot-based field data.

Across all sites in this study, a significant negative relationship was observed between UAV-LiDAR detection rate and plot-based stem density of stems taller than 1.3 m. At sites with plot-based mean densities below 4000 sph, UAV-LiDAR captured between 62% and 79% of the plot-based mean density; however, at sites where mean stem density exceeded

4000 sph, UAV-LiDAR captured only 14% to 51% of the plot-based estimates, depending on site conditions. Density estimates from ALS were consistently lower than those from UAV-LiDAR, capturing only 1% to 21% of the plot-based mean density. This result was expected given the lower horizontal and vertical point densities of ALS data, which reduce the distinguishability of individual tree crowns within the point cloud [27]. Unlike the UAV-LiDAR, ALS detection rates were not significantly correlated with plot-based density, likely because most sites exceeded density thresholds at which accurate individual tree detection from lower point density ALS data is feasible. The close spacing and overlapping crowns characteristic of high-density stands presents a substantial challenge for individual tree isolation from LiDAR, and increasing canopy cover further reduces detection accuracy [13,28]. Subcanopy species are poorly represented due to occlusion by the overstory [29,30]. While previous studies have also reported declining individual tree detection accuracy with increasing stem density [13,22,26,31], the highest densities examined in those studies were approximately 2000 sph. In contrast, reclaimed wellsites often have higher stem densities with one study reporting a mean of 2339 trees per hectare across 30 certified wellsites in Alberta [32]. In the current study, woody stem densities (>1.3 m) at the OSE sites and wellsites frequently exceeded 3000 sph, with several sites over 10,000 sph, representing stand conditions that are largely absent from existing LiDAR literature focused primarily on managed forests or plantations (Table 5).

Table 5. Individual tree detection accuracies from other studies using LiDAR data showing the segmentation method used, point or pulse density, forest type, tree height (mean and range or SD) and density (mean and range) of each study.

Study	Point or Pulse Density (m^{-2})	Forest Type	Tree Height (m)	Density (sph)	Tree Detection Accuracy	Segmentation Method
Du & Pang, 2024 [33]	243 points	Mixed conifer plantation with sapling understory	<3.5 m	845	Matching rate: 82%	Adaptive-mean-shift-based clustering algorithm
Watt et al., 2024 [34]	15,966 points	Conifer plantation	17.7 (11.4–21.5)	456	Recall: 0.98 *	CHM-based Local maxima filter
Li et al., 2023 [35]	298 points	Deciduous plantation	15	1400	Recall: 0.61 *	Pit-free CHM generation than initial WS segmentation and fine segmentation using the optimized CCE
	3295 points	Mixed plantation	18	1000	Recall: 0.75 *	
	1636 points	Conifer plantation	21	500	Recall: 0.92 *	
	1473 points	Conifer plantation	15	1000	Recall: 0.71 *	
	3976 points	Conifer plantation	16	1000	Recall: 0.89 *	
Sparks et al., 2022 [26]	22 pulses	Mixed conifer temperate forest	15.9 (6.1–40.9)	543 (18–1847)	Recall: 0.13–0.62 **	Seven methods compared (point-cloud, raster-based and hybrid)
Hao et al., 2022 [36]	200 points	Conifer plantation	22.0 (13.3–28.9)	653 (489–855)	Recall: 0.86	Hierarchical Region-Merging Algorithm
		Conifer plantation	22.2 (14.0–28.0)	1058 (933–1367)	Recall: 0.83	
		Conifer plantation	15.6 (6.1–21.3)	2091 (1722–2577)	Recall: 0.78	
		Mixed plantation	13.9 (5.7–20.0)	1849 (1612–2224)	Recall: 0.78	

Table 5. *Cont.*

Study	Point or Pulse Density (m^{-2})	Forest Type	Tree Height (m)	Density (sph)	Tree Detection Accuracy	Segmentation Method
Donager et al., 2021 [13]	19.8	Conifer plantation	7.6–28.5	25–1361	Detection rate: 68.3%	Dalponte and Coomes algorithm
Vauhkonen et al., 2012 [22]	7 and 16 points	Conifer stands and Deciduous stands	Not reported	664 (347) and 733 (331)	Detection rate: 49–101% ** (mean 75%)	Six different algorithms
	7.4 points	Mixed boreal	Not reported	1093 (485)	Detection rate: 45–68% ** (mean 54%)	Six different algorithms
	30 points	Mixed boreal	Not reported	610 (253)	Detection rate: 65–86% ** (mean 73%)	Six different algorithms
Yu et al., 2011 [31]	1.8–3.4 points	Mixed boreal, 24% broadleaf	16.5 (4.4–34.6)	400–2000	Detection rate: 43–96% (mean 69%)	Laser derived features and random forests algorithm

* = Described as $R_{match.}$ ** = Depending on algorithm used.

Forest type further influences tree detection accuracy for both UAV-LiDAR and ALS. Species with irregular canopy shapes or multiple stems, including many deciduous species and shrubs, pose challenges for individual tree detection algorithms [27]. Higher accuracies of LiDAR-derived forest attributes have been consistently reported in conifer-dominated stands relative to deciduous or mixed forests [27,37], and increasing structural complexity in mixed stands further reduces detection performance [38]. Accordingly, the mixed species composition and high proportion of deciduous tree and shrub species (58% to 99%) at these sites examined here likely contributed to the systematic underestimation of woody stem density in LiDAR-derived estimate relative to field data.

Tree heights from LiDAR data are widely used in forest inventories, and numerous studies have demonstrated strong agreement between LiDAR-derived and field measured individual tree heights [9,31,39]. In this study, reference tree heights from UAV-LiDAR showed excellent alignment with field measurements (R^2 = 0.98 and RMSE = 23 cm). However, on the site scale, when analyses were restricted to woody stems taller than 1.3 m, both UAV-LiDAR and ALS estimates showed a slight tendency to overestimate mean height relative to plot-based values. This slight overestimation is likely attributable to two main factors: (1) the under-detection of shorter stems in high density areas, which biased LiDAR-derived height distributions towards taller individuals and (2) the difference in spatial extent between full-coverage LiDAR surveys and the limited areas sampled by field plots. The site-wide LiDAR data captures edge environments, where trees may be taller due to earlier natural ingress from the adjacent forest, whereas plot-based measurements may underrepresent these edge effects. Despite this tendency towards overestimation, mean heights and associated SD derived from both UAV-LiDAR and ALS estimates were generally consistent with plot-based estimates. The finding that UAV-LiDAR and ALS surveys closely represented the site's mean height despite capturing lower stem densities than field plots indicates that the heights of the un-detected stems were likely similar to those of the detected stems, at least for stems taller than 1.3 m included in the LiDAR analysis.

4.3. Implications for LiDAR in Reclamation Certification

The omission of low-stature vegetation, which can often be a large component of the vegetation on reclaimed sites, is an important limitation for the application of LiDAR data in reclamation certification. If LiDAR-based methods are to be used, a minimum time since planting may be required before certification to ensure sufficient vegetation development that is detectable from LiDAR.

The reduced stem detection rates in high-density stands represents another important limitation for the application of LiDAR data in reclamation certification; however, the findings of this study highlight the utility of LiDAR as a potential screening tool. When LiDAR-derived stem density estimates meet minimum certification criteria, the actual stem densities are likely higher once undetected small and clustered stems are considered. Conversely, sites that fail to meet density threshold based on LiDAR data alone may warrant targeted field verification. In this study, UAV-LiDAR detection rates were low (14% to 53% of mean plot density) where the density of stems taller than 1.3 m exceeded 4000 sph. Because 5000 sph is the minimum density requirement for natural recovery sites, the observed limitations in individual tree segmentation at high stem densities suggests that LiDAR may be insufficient for direct certification assessment without supporting field data.

The selection of ecological indicators is an important consideration in evaluating restoration success [5]. It should be noted that high densities of low-stature shrubs, such as the rose and raspberry observed in this study, may not necessarily indicate long-term reclamation success. Lupardus et al. [32] identified canopy cover and live tree basal area as important ecological indicators of recovery on wellsites. Reclamation certification criteria emphasizing tree establishment is a more meaningful indicator of progress toward a forested end state [40]. In this context, trees taller than 1.3 m may represent a more ecologically relevant metric for assessing recovery trajectory towards forest development with the added benefit of being more reliably detected by LiDAR for monitoring.

LiDAR data also offer clear advantages for site-scale assessment by providing spatially explicit information on vegetation distribution and structure. In this study, LiDAR-derived tree distributions were used to interpret discrepancies in woody species attribute estimates among different plot types. Spatial patterns derived from LiDAR visually confirmed the association between heterogenous woody species distributions and failure of randomly placed plots to meet minimum density criteria. Additionally, LiDAR surveys provide complete spatial coverage of disturbed areas, enabling characterization of recovery patterns that cannot be achieved through plot-based sampling alone. While conventional field plots in this study sampled only 0.8% to 1.9% of site area, LiDAR captured vegetation attributes across entire sites, including spatial heterogeneity and localized areas of poor recovery.

Aerial surveys have long been used in forestry to stratify zones of differential regeneration [41], and ALS-derived metrics are increasing applied in forest inventories to guide stratification and sampling strategies [42]. Similarly, LiDAR data could support reclamation certification by informing adaptive sampling designs, focusing field effort in heterogeneous or marginal areas while reducing sampling intensity in uniformly recovering zones.

4.4. Limitations and Recommendations

A key limitation of this study is the temporal misalignment between datasets: the ALS LiDAR data were collected in 2022–2023, whereas field surveys were conducted in 2025, resulting in a two- to three-year gap. This temporal discrepancy may contribute to the underestimation of woody stem counts from ALS LiDAR relative to plot data, as individuals measuring < 1.3 m during the ALS LiDAR acquisition could have grown beyond this threshold by the time of field sampling. Similarly, this temporal offset would be expected to produce an underestimation of tree height from ALS LiDAR relative to field measurements. Therefore, the observed overestimation of height derived from ALS LiDAR is likely even more pronounced than reported.

There is a need for improved individual tree detection from LiDAR in areas of high stem density. Future studies could explore improving individual tree detection in dense stands, potentially with training data from higher density stands. Furthermore, individual

tree detection from ALS LiDAR was limited in this study; however, ongoing advancements in LiDAR technology, such as higher point densities and improved sensor configurations, are expected to substantially improve detection accuracy. Integrating these emerging technologies with more representative training datasets is likely to enhance performance in dense forest environments.

5. Conclusions

This study evaluated woody vegetation recovery on certified reclaimed OSE sites and wellsites using a combination of field-based sampling and LiDAR-derived metrics. Across all sites, woody stem density and height estimates from randomly placed plots were comparable to those derived from plots placed using professional judgement. However, at sites exhibiting heterogenous recovery, plot placement using professional judgement tended to overestimate woody density relative to estimates obtained from larger sampling areas, indicating increased sensitivity of plot placement effects under spatially variable vegetation conditions. In contrast, random plot estimates aligned more closely with increased sampling approaches, suggesting that random sampling provides a more representative assessment of site conditions, if site-level rather than plot-level criteria are emphasized.

Both UAV-LiDAR and ALS underestimated site-level woody stem densities and slightly overestimated site-level mean height, reflecting limitations in detecting small woody vegetation and challenges in segmenting dense clusters of vegetation. Detection rates were substantially lower for ALS than UAV-LiDAR. Despite these limitations, UAV-LiDAR provided valuable spatial and structural information, supporting its use as a screening tool to identify sites unlikely to require intensive field surveys and to guide targeted field verification where necessary. Overall, integrating randomized field sampling with UAV-LiDAR data offers a promising pathway to improve the accuracy, efficiency, and transparency of reclaimed wellsite certification.

Author Contributions: Conceptualization, D.D. and A.V.D.; methodology, D.D., A.V.D., D.M. and C.S.; software, D.M.; validation, D.M. and A.V.D.; formal analysis, A.V.D. and D.M.; data curation, A.V.D. and D.M.; writing—original draft preparation, A.V.D., D.M. and C.S.; writing—review and editing, A.V.D., D.M., C.S. and D.D.; visualization, D.M.; supervision, D.D.; project administration, D.D.; funding acquisition, D.D. All authors have read and agreed to the published version of the manuscript.

Funding: This research was funded by Natural Resources Canada Office of Energy Research and Development, grant #CFS-23-101.

Data Availability Statement: Data available upon request.

Acknowledgments: We would like to acknowledge the Forest Resource Improvement Association of Alberta (FRIAA) and Alberta Biodiversity Monitoring Institute (ABMI) for sharing the ALS data. We would also like to acknowledge Carrie Robertson for her help with site selection, Elizabeth Friel for her assistance in the field and Zhouxin Xi for his assistance with the TreeAIBox plugin.

Conflicts of Interest: The authors declare no conflicts of interest.

Abbreviations

The following abbreviations are used in this manuscript:

ABMI	Alberta biodiversity monitoring institute
AER	Alberta energy regulator
ALS	Aerial laser scanning
DSA	Detailed site assessment
LiDAR	Light detecting and ranging

OSE	Oil sand exploration
PJ	Professional judgement plot type (10 m^2)
R^2	Coefficient of determination
R	Random plot type (10 m^2)
R+	Additional random plot type (10 m^2)
RL	Large random plot type (50 m^2)
RMSE	Root mean square error
SD	Standard deviation
SE	Standard error
sph	Stems per hectare
UAV	Uncrewed aerial vehicle

Appendix A

Table A1. Site information including the number of grid areas, disturbance type (OSE = Oil Sand Exploration), revegetation method, year of abandonment, and year of certification.

Site	# of Grid Areas	Disturbance Type	Revegetation Method	Year of Abandonment	Year of Certification
1	9	OSE	Natural Recovery	2010	2024
2	9	Wellsite	Planted	2018	2023
3	9	Wellsite	Natural Recovery	2013	2024
4	9	Wellsite	Planted	2006	2025
5	4	Wellsite	Natural Recovery	2004	2023
6	4	OSE	Natural Recovery	2010	2023
7	4	Wellsite	Natural Recovery	2010	2023
8	4	Wellsite	Natural Recovery	2011	2023
9	4	Wellsite	Natural Recovery	2011	2022
10	4	OSE	Planted	2012	2023
11	4	OSE	Planted	2012	2023
12	4	OSE	Planted	2015	2022
13	4	Wellsite	Planted	2018	2024
14	4	OSE	Natural Recovery	2018	2023

Table A2. Deciduous proportion and dominant species at each site.

Site	% Deciduous	Dominant Woody Species	Dominant Conifer
1	89	*Rubus idaeus*, *Rosa acicularis*, *Populus balsamifera*	*Picea glauca*
2	99	*Rubus idaeus*, *Rosa acicularis*, *Populus balsamifera*	*Picea glauca*
3	97	*Rubus idaeus*, *Rosa acicularis*, *Populus balsamifera*	*Picea glauca*
4	99	*Salix* sp., *Populus balsamifera*, *Picea glauca*	*Picea glauca*
5	91	*Rosa acicularis*, *Rubus idaeus*, *Ribes* sp.	*Picea glauca*
6	85	*Salix* sp., *Populus balsamifera*, *Betula papyrifera*	*Larix laricina*
7	97	*Rosa acicularis*, *Rubus idaeus*, *Salix* sp.	*Picea glauca*
8	97	*Populus balsamifera*, *Salix* sp., *Betula papyrifera*	*Picea glauca*
9	97	*Betula papyrifera*, *Salix* sp., *Populus balsamifera*	*Picea glauca*
10	58	*Salix* sp., *Rubus idaeus*, *Rosa acicularis*	*Picea glauca*
11	71	*Salix* sp., *Populus balsamifera*, *Rubus idaeus*	*Picea glauca*
12	96	*Salix* sp., *Populus balsamifera*, *Picea glauca*	*Picea glauca*
13	62	*Alnus alnobetula*, *Salix* sp., *Pinus banksiana*	*Pinus banksiana*
14	71	*Salix* sp., *Populus tremuloides*, *Betula papyrifera*	*Pinus banksiana*

Table A3. Summary of ALS data specifications acquired by ABMI.

Parameter	Conklin Study Area (Sites 2,7,8,9,12, and 13)	Conklin Study Area (Sites 5 and 14)	Cold Lake Study Area
Dates of Acquisition	Jun 5–Aug 29, 2022	Jul 2; Aug 11; Sep 3–4, 10–11, 2022	Jul 4, 16, 21, 29–31; Aug 1–2, 13–14, 17, 26; Sep 16–17, 2023
Lidar Sensor	Riegl VQ-1560ii	ALTM Galaxy T2000	
Number of Returns Per Pulse	-	1–8	
Point Density (points per m^2)	12	24	29
Scan Angle or Field of View (degrees)	60	+/−22	+/−25
Swath Width (m)	-	1400	1150
Swath Overlap (%)	50	25	30

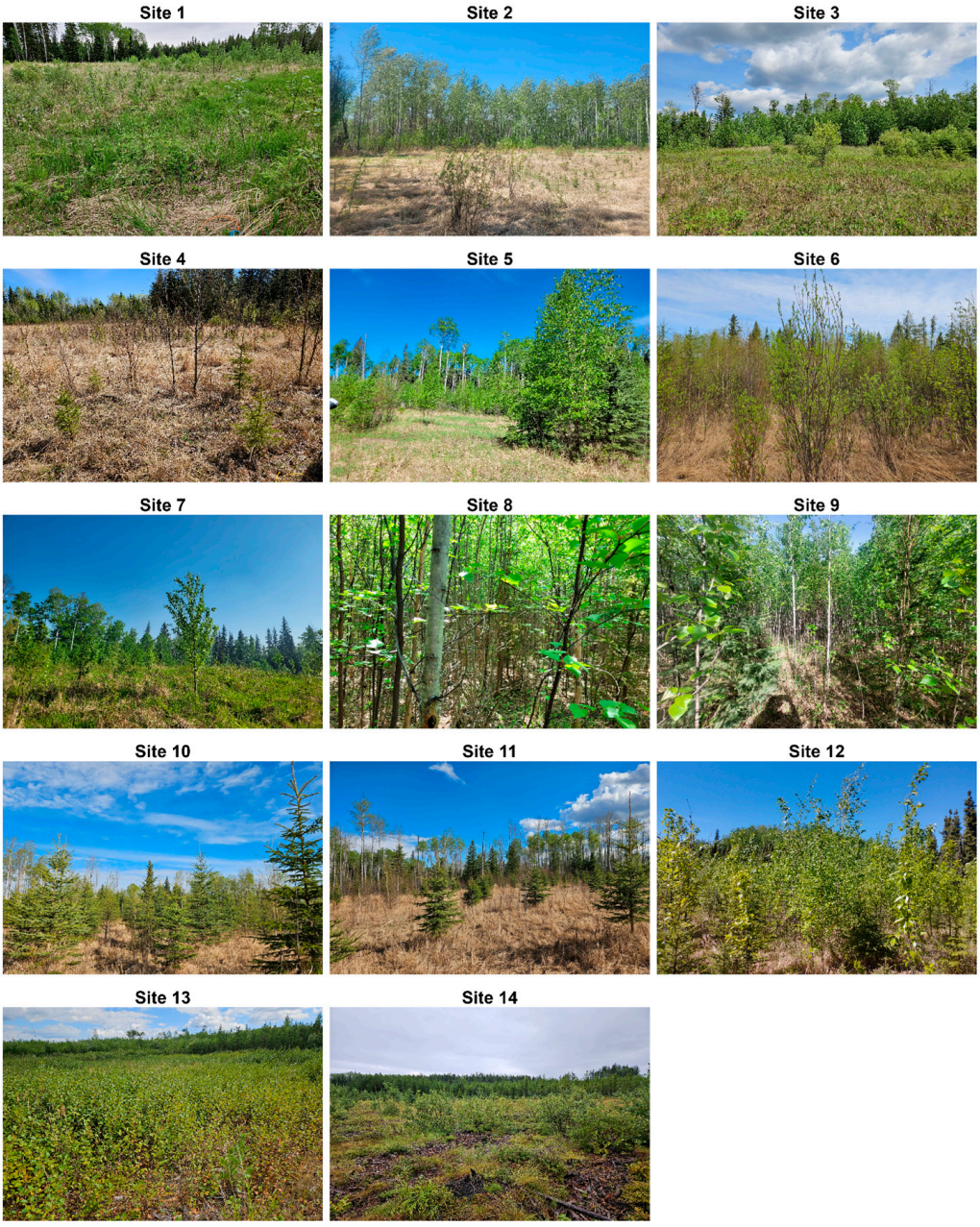


Figure A1. Photographs of reclaimed sites.

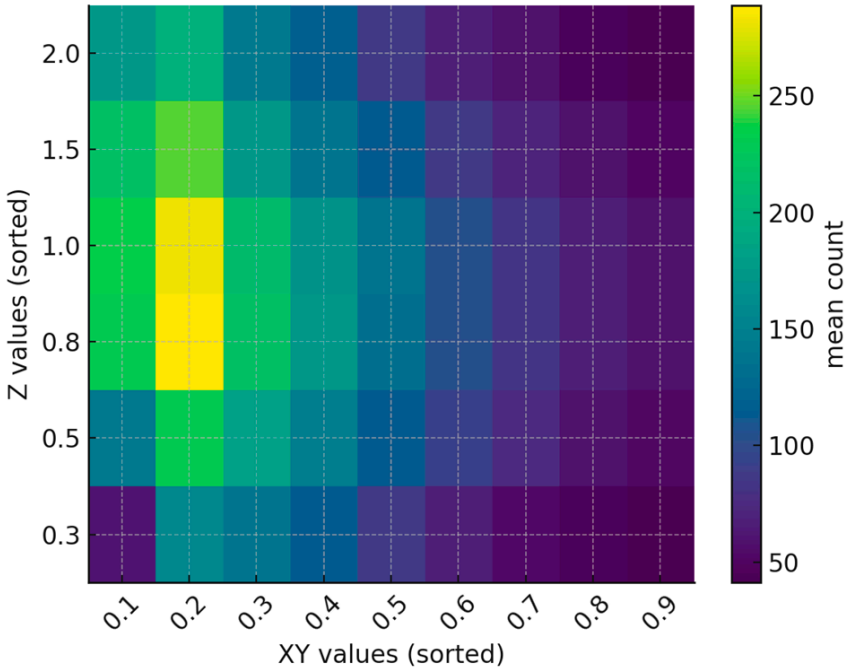


Figure A2. Heatmap of mean tree detection rates across XY–Z combinations of TreeAIBox plugin for ALS dataset from eight sites.

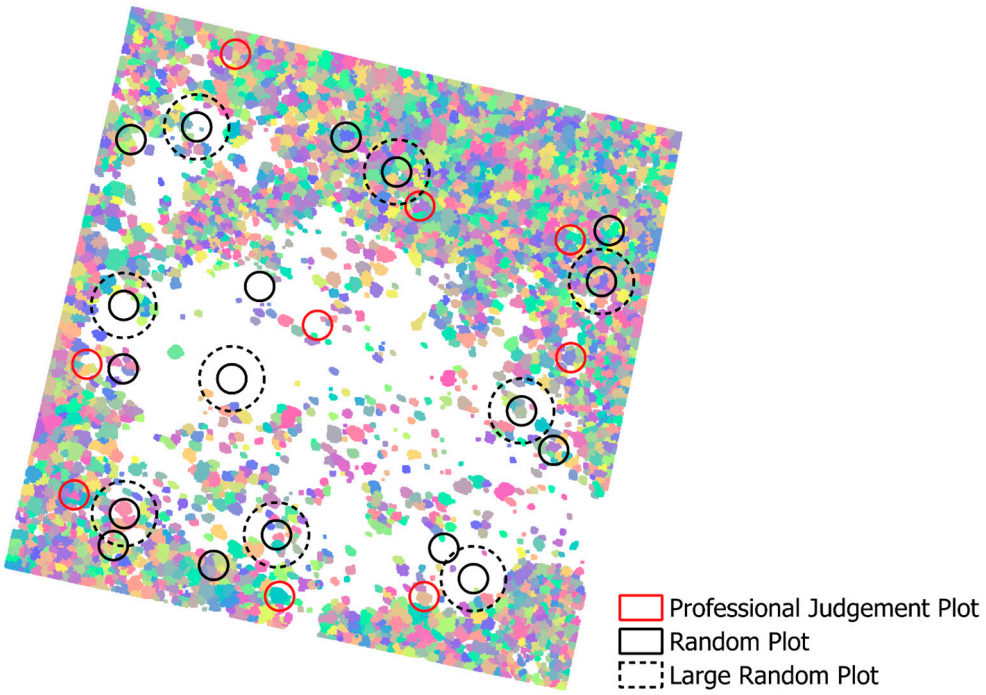


Figure A3. Locations of UAV-LiDAR-detected trees across Site 2. Each isolated tree is depicted in a different colour. Red circles indicate professional judgement plots (10 m^2), black circles indicate random plots (10 m^2) and dashed black circles indicate larger random plots (50 m^2) area.

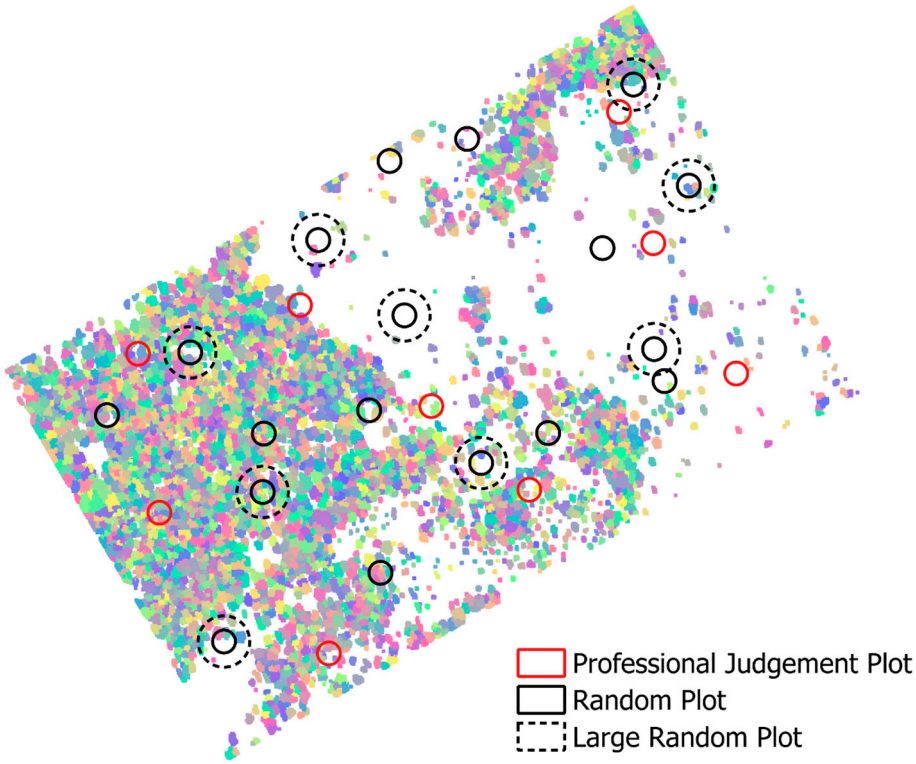


Figure A4. Locations of UAV-LiDAR-detected trees across Site 4. Each isolated tree is depicted in a different colour. Red circles indicate professional judgement plots (10 m^2), black circles indicate random plots (10 m^2) and dashed black circles indicate larger random plots (50 m^2) area.

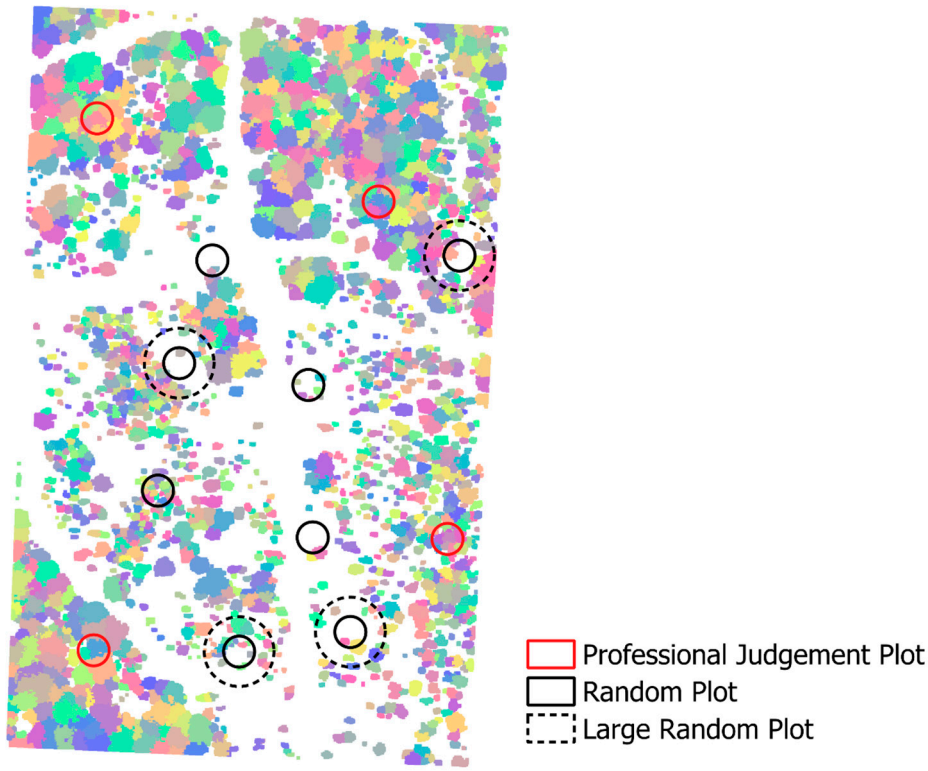


Figure A5. Locations of UAV-LiDAR-detected trees across Site 5. Each isolated tree is depicted in a different colour. Red circles indicate professional judgement plots (10 m^2), black circles indicate random plots (10 m^2) and dashed black circles indicate larger random plots (50 m^2) area.

Table A4. Model specifications for generalized linear mixed effects models and ANOVA results indicating significant effects ($p < 0.05$) for (x^2) tests.

Plot Type Comparison	Group	Variable	Fixed Effect	Random Effect	Distribution	Varying Dispersion Parameter	x^2	Df	p
PJ, R	Woody	Density (sph)	Plot type	Site	Tweedie (log link)	None	1.8	1	0.17
PJ, R	Woody	Height (m)	Plot type	Site	Gamma (log link)	None	2.6	1	0.11
PJ, R	Woody > 1.3 m	Density (sph)	Plot type	Site	Tweedie (log link)	Site	0.48	1	0.48
PJ, R	Woody > 1.3 m	Height (m)	Plot type	Site	Gamma (log link)	Site * Plot	0.95	1	0.33
PJ, R, R+, RL	Woody	Density (sph)	Plot type	Site	Tweedie (log link)	None	28.6	3	<0.001
PJ, R, R+, RL	Woody	Height (m)	Plot type	Site	Gamma (log link)	None	4.35	3	0.23
PJ, R, R+, RL	Woody > 1.3 m	Density (sph)	Plot type	Site	Tweedie (log link)	Plot	19.87	3	<0.001
PJ, R, R+, RL	Woody > 1.3 m	Height (m)	Plot type	Site *	Gamma (log link)	None	3.46	3	0.33

* Site 5 excluded from dataset for this model for improved model residuals.

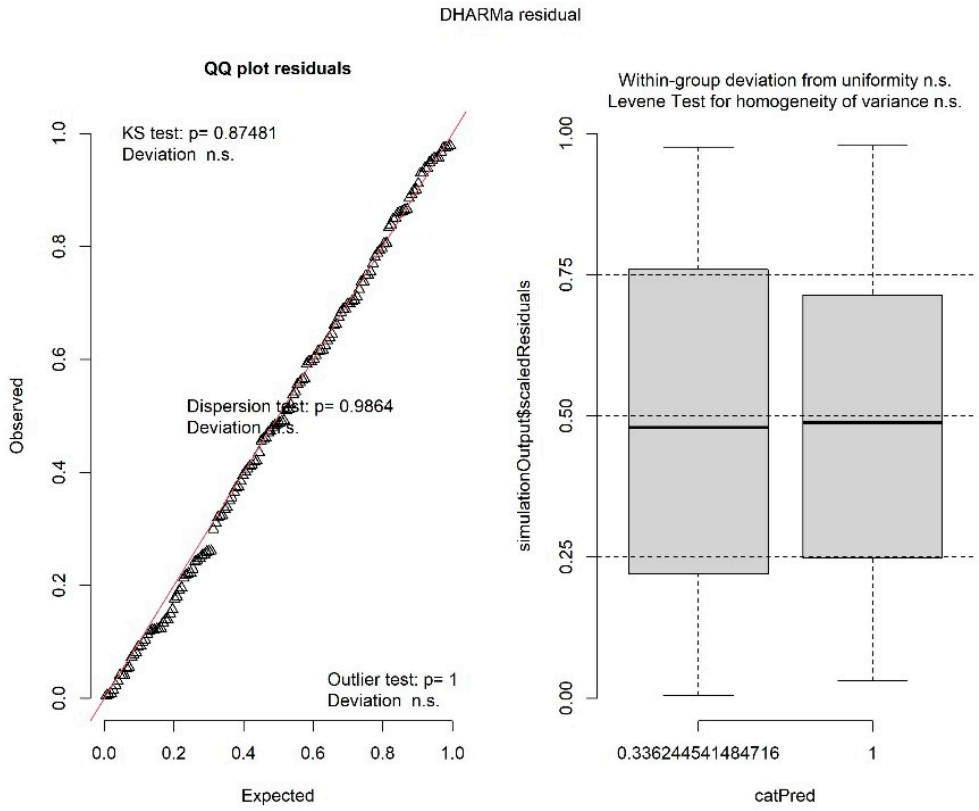


Figure A6. Model diagnostics for the generalized linear mixed-effect model of woody species density from professional judgement vs. random placement plots.

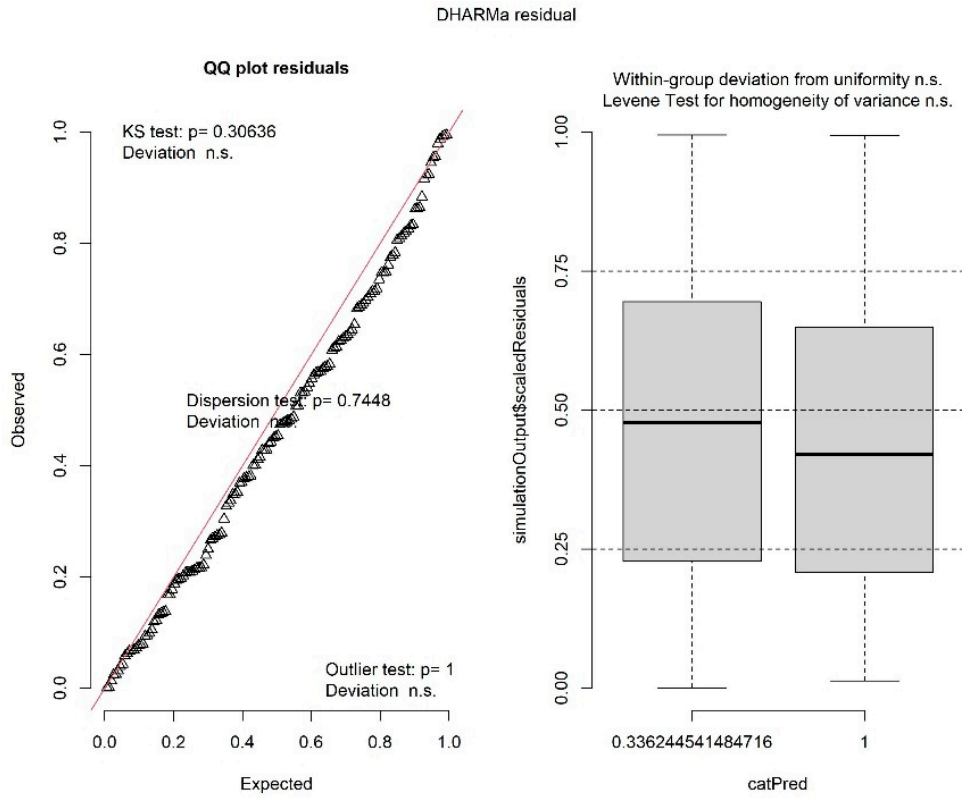


Figure A7. Model diagnostics for the generalized linear mixed-effect model of woody species height from professional judgement vs. random placement plots.

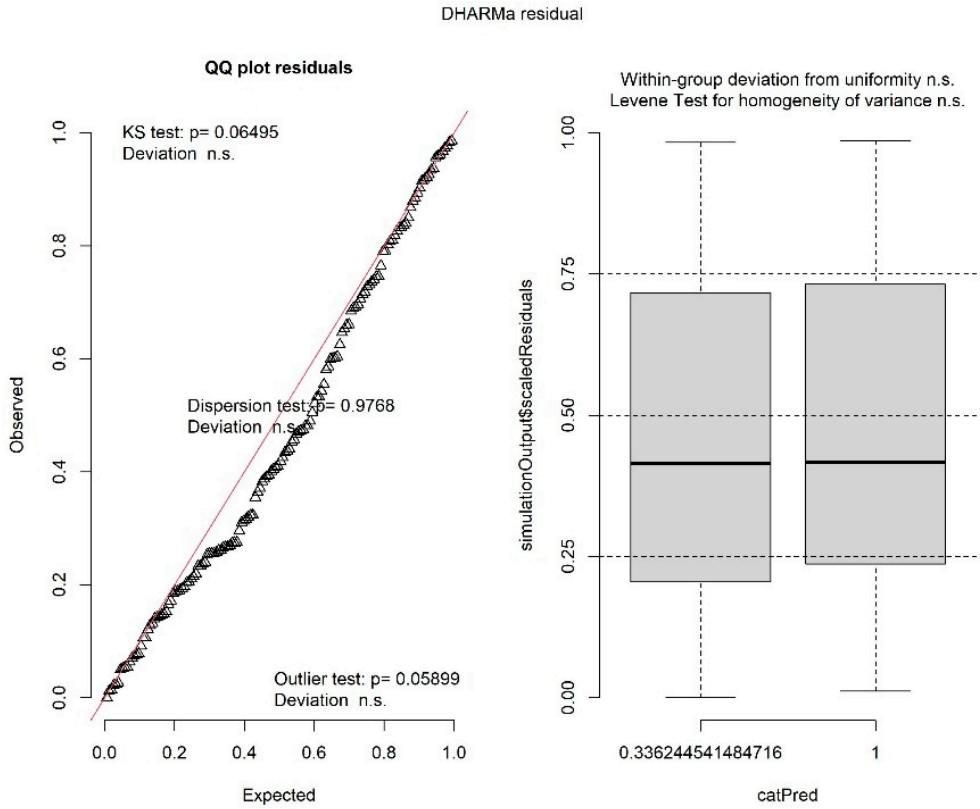


Figure A8. Model diagnostics for the generalized linear mixed-effect model of woody species taller than 1.3 m density from professional judgement vs. random placement plots.

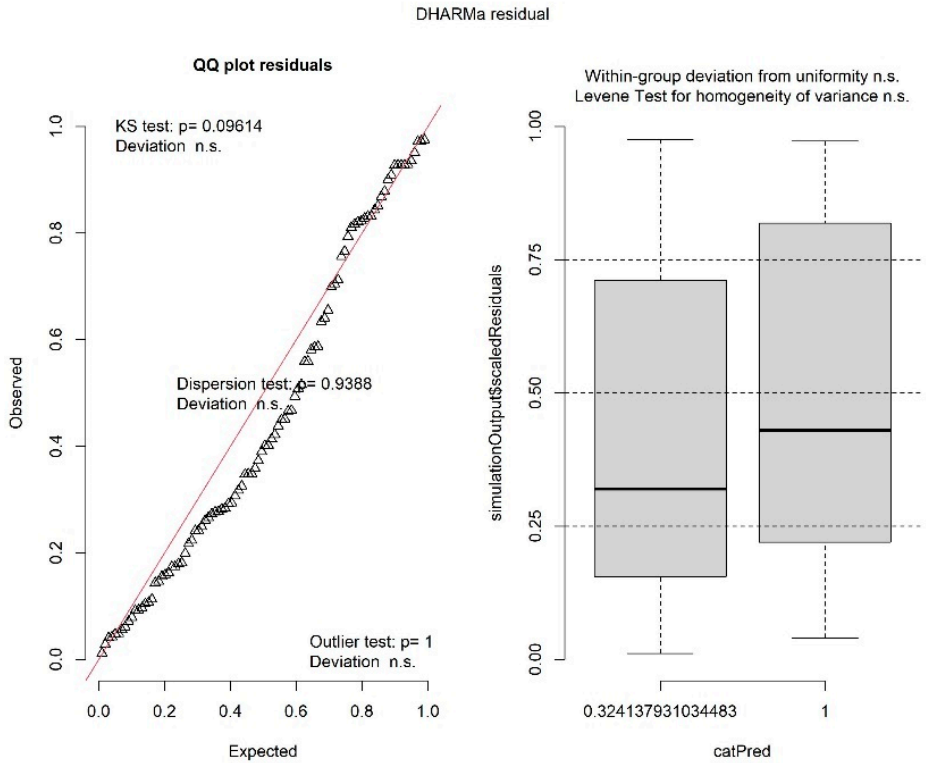


Figure A9. Model diagnostics for the generalized linear mixed-effect model of woody species taller than 1.3 m height from professional judgement vs. random placement plots.

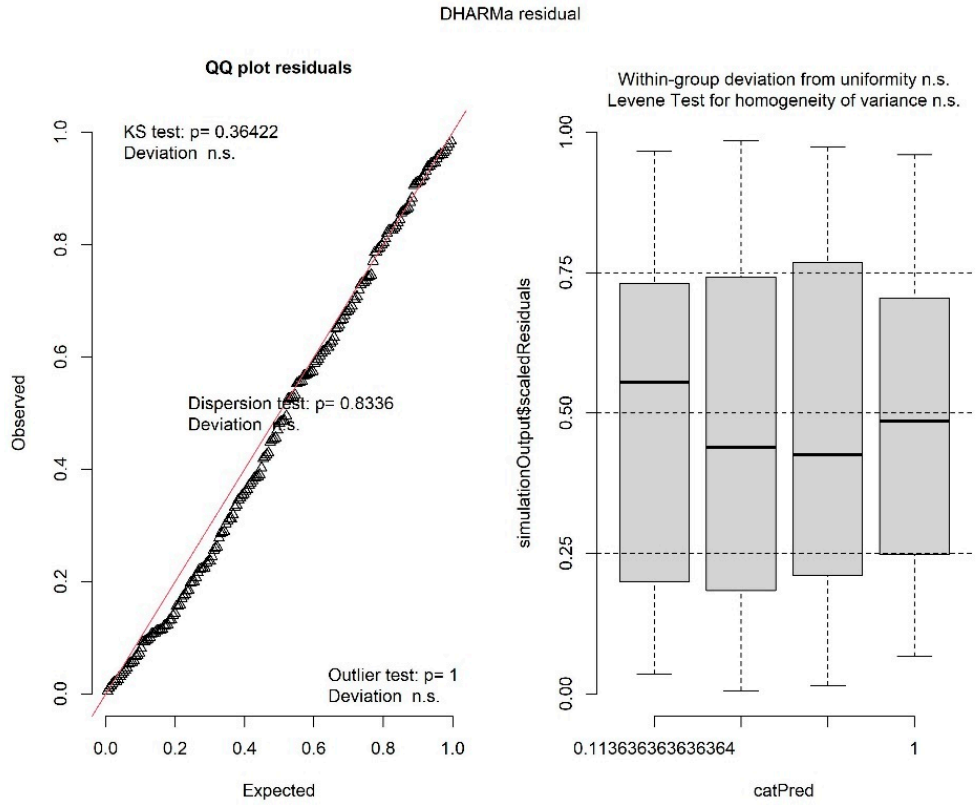


Figure A10. Model diagnostics for the generalized linear mixed-effect model of woody species density from professional judgement, random, additional random, and large random plots.

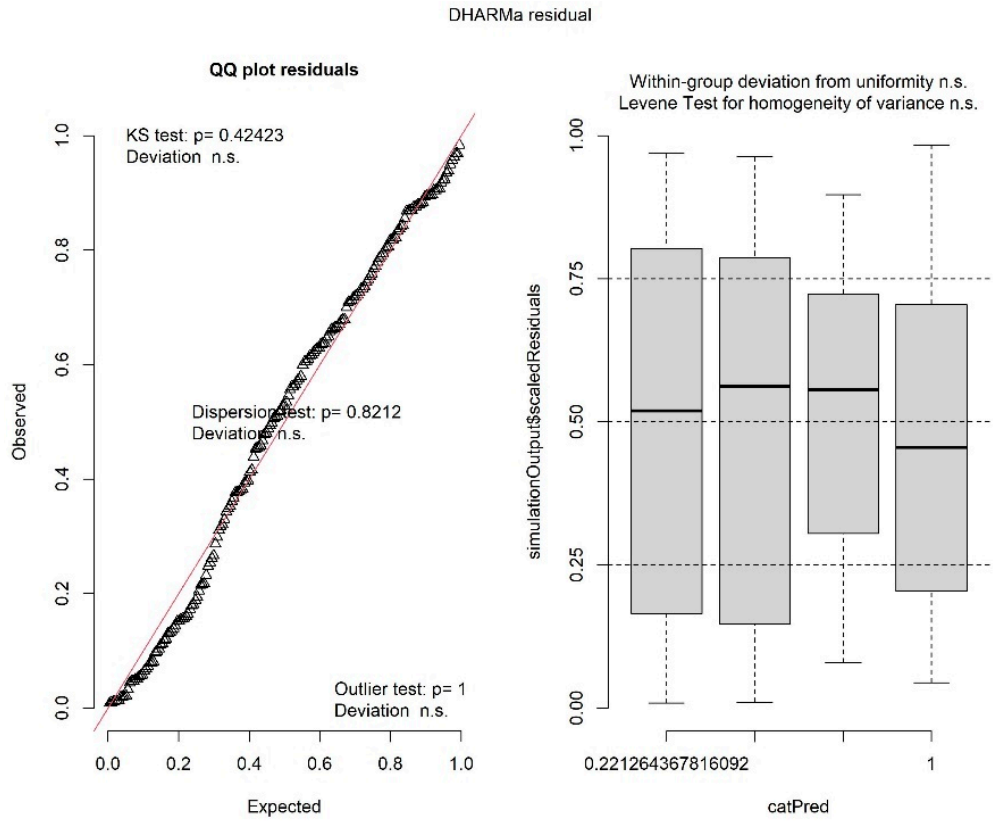


Figure A11. Model diagnostics for the generalized linear mixed-effect model of woody species height from professional judgement, random, additional random, and large random plots.

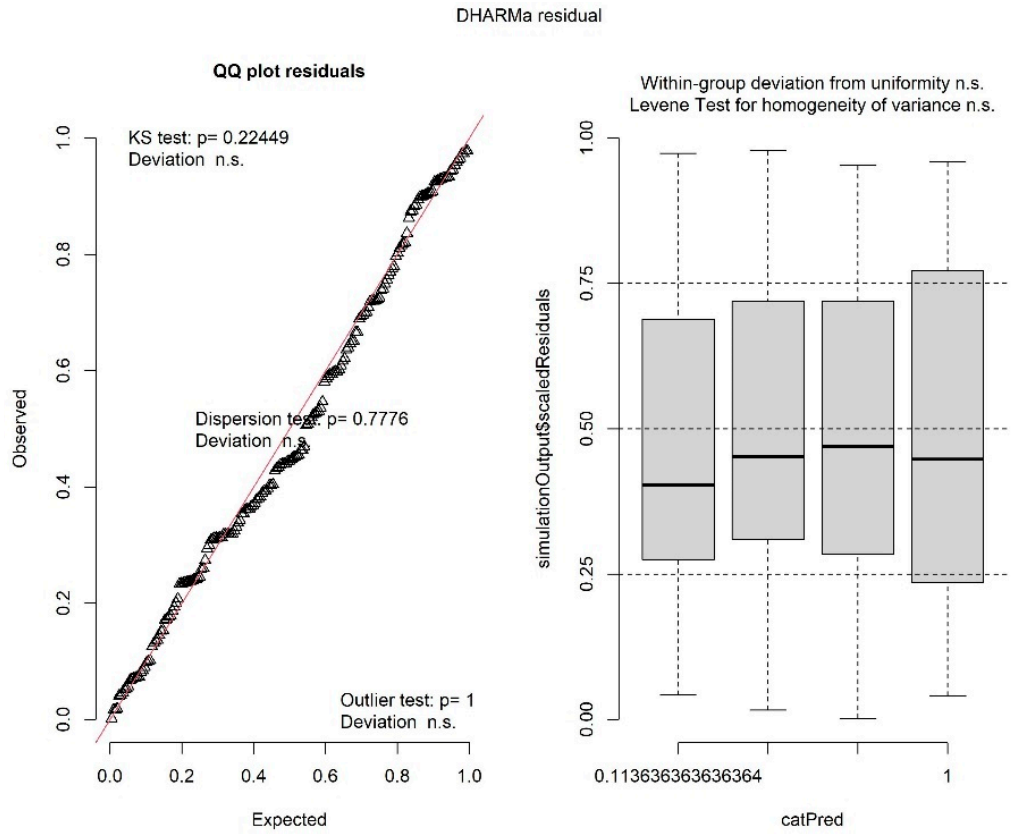


Figure A12. Model diagnostics for the generalized linear mixed-effect model of woody species taller than 1.3 m density from professional judgement, random, additional random, and large random plots.

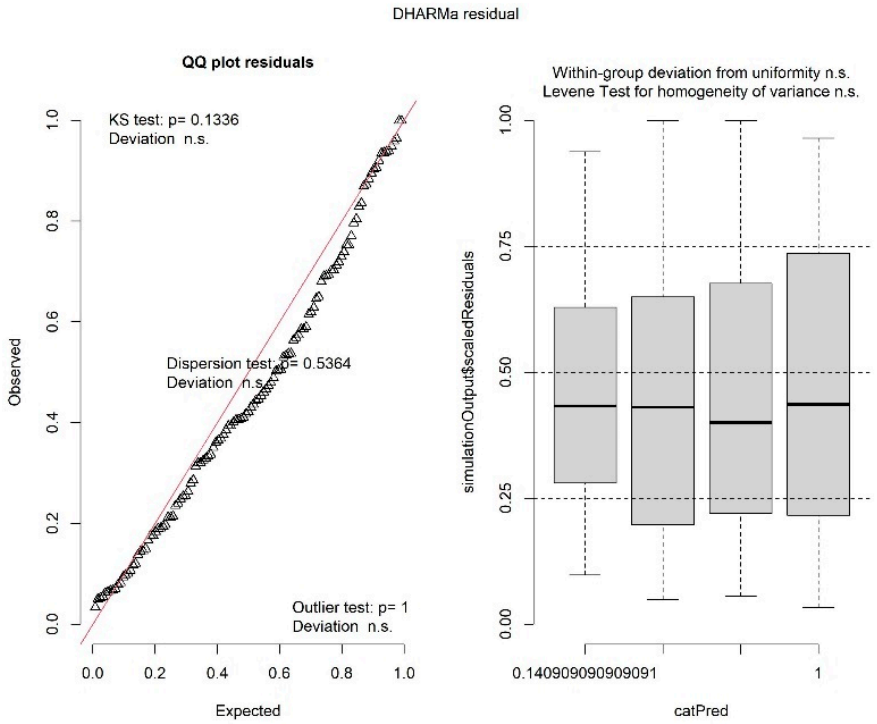


Figure A13. Model diagnostics for the generalized linear mixed-effect model of woody species taller than 1.3 m height from professional judgement, random, additional random, and large random plots.

References

1. Alberta Energy Regulator Well Status. 2025. Available online: https://static.aer.ca/prd/documents/sts/ST98/2025/Alberta-Energy-Outlook_report.pdf (accessed on 15 April 2026).
2. Government of Alberta. *Environmental Protection and Enhancement Act*; King's Printer: Edmonton, AB, Canada, 2025.
3. Government of Alberta. Environment and Sustainable Resource Development. In *2010 Reclamation Criteria for Wellsites and Associated Facilities for Forested Lands*; Environment and Parks: Edmonton, AB, Canada, 2013; p. 81.
4. Environment and Parks. *Reclamation Criteria for Wellsites and Associated Facilities for Peatlands*; Environment and Parks: Edmonton, AB, Canada, 2017; p. 142.
5. Prach, K.; Durigan, G.; Fennessy, S.; Overbeck, G.E.; Torezan, J.M.; Murphy, S.D. A Primer on Choosing Goals and Indicators to Evaluate Ecological Restoration Success. *Restor. Ecol.* **2019**, *27*, 917–923. [CrossRef]
6. Ruiz-Jaen, M.C.; Mitchell Aide, T. Restoration Success: How Is It Being Measured? *Restor. Ecol.* **2005**, *13*, 569–577. [CrossRef]
7. Williams, B.K.; Brown, E.D. Sampling and Analysis Frameworks for Inference in Ecology. *Methods Ecol. Evol.* **2019**, *10*, 1832–1842. [CrossRef]
8. Gibbons, P.; Freudenberger, D. An Overview of Methods Used to Assess Vegetation Condition at the Scale of the Site. *Ecol. Manag. Restor.* **2006**, *7*, S10–S17. [CrossRef]
9. Movchan, D.; Xi, Z.; Van Dongen, A.; Selvaraj, C.; Degenhardt, D. UAV-Based Wellsite Reclamation Monitoring Using Transformer-Based Deep Learning on Multi-Seasonal LiDAR and Multispectral Data. *Remote Sens.* **2025**, *17*, 3440. [CrossRef]
10. Xi, Z.; Degenhardt, D. A New Unified Framework for Supervised 3D Crown Segmentation (TreeisoNet) Using Deep Neural Networks across Airborne, UAV-Borne, and Terrestrial Laser Scans. *ISPRS Open J. Photogramm. Remote Sens.* **2025**, *15*, 100083. [CrossRef]
11. Hird, J.; Montaghi, A.; McDermid, G.; Kariyeva, J.; Moorman, B.; Nielsen, S.; McIntosh, A. Use of Unmanned Aerial Vehicles for Monitoring Recovery of Forest Vegetation on Petroleum Well Sites. *Remote Sens.* **2017**, *9*, 413. [CrossRef]
12. White, J.C.; Tompalski, P.; Bater, C.W.; Wulder, M.A.; Fortin, M.; Hennigar, C.; Robere-McGugan, G.; Sinclair, I.; White, R. Enhanced Forest Inventories in Canada: Implementation, Status, and Research Needs. *Can. J. For. Res.* **2025**, *55*, 1–37. [CrossRef]
13. Donager, J.J.; Sánchez Meador, A.J.; Blackburn, R.C. Adjudicating Perspectives on Forest Structure: How Do Airborne, Terrestrial, and Mobile Lidar-Derived Estimates Compare? *Remote Sens.* **2021**, *13*, 2297. [CrossRef]
14. Alberta Parks. *Natural Regions and Subregions of Alberta. A Framework for Alberta's Parks*; Alberta Tourism, Parks and Recreation: Edmonton, AB, Canada, 2015; p. 72.
15. Government of Canada. *Canadian Climate Normals 1991–2020*; Government of Canada: Cold Lake, AB, Canada, 2020.
16. Brandt, J.P. The Extent of the North American Boreal Zone. *Environ. Rev.* **2009**, *17*, 101–161. [CrossRef]

17. *Alberta Energy Regulator Application Query*; Alberta Energy Regulator: Calgary, AB, Canada, 2025.
18. Rodríguez-Puerta, F.; Gómez-García, E.; Martín-García, S.; Pérez-Rodríguez, F.; Prada, E. UAV-Based LiDAR Scanning for Individual Tree Detection and Height Measurement in Young Forest Permanent Trials. *Remote Sens.* **2021**, *14*, 170. [CrossRef]
19. R Core Team. *R: A Language and Environment for Statistical Computing*; R Foundation of Statistical Computing: Vienna, Austria, 2025.
20. Fisher, J.I.; Hurtt, G.C.; Thomas, R.Q.; Chambers, J.Q. Clustered Disturbances Lead to Bias in Large-scale Estimates Based on Forest Sample Plots. *Ecol. Lett.* **2008**, *11*, 554–563. [CrossRef] [PubMed]
21. Goslee, S.C. Behavior of Vegetation Sampling Methods in the Presence of Spatial Autocorrelation. *Plant Ecol.* **2006**, *187*, 203–212. [CrossRef]
22. Vauhkonen, J.; Ene, L.; Gupta, S.; Heinzel, J.; Holmgren, J.; Pitkanen, J.; Solberg, S.; Wang, Y.; Weinacker, H.; Hauglin, K.M.; et al. Comparative Testing of Single-Tree Detection Algorithms under Different Types of Forest. *Forestry* **2012**, *85*, 27–40. [CrossRef]
23. Alvites, C.; Marchetti, M.; Lasserre, B.; Santopuoli, G. LiDAR as a Tool for Assessing Timber Assortments: A Systematic Literature Review. *Remote Sens.* **2022**, *14*, 4466. [CrossRef]
24. Næsset, E.; Nelson, R. Using Airborne Laser Scanning to Monitor Tree Migration in the Boreal–Alpine Transition Zone. *Remote Sens. Environ.* **2007**, *110*, 357–369. [CrossRef]
25. Næsset, E.; Bjerknes, K.-O. Estimating Tree Heights and Number of Stems in Young Forest Stands Using Airborne Laser Scanner Data. *Remote Sens. Environ.* **2001**, *78*, 328–340. [CrossRef]
26. Sparks, A.M.; Corrao, M.V.; Smith, A.M.S. Cross-Comparison of Individual Tree Detection Methods Using Low and High Pulse Density Airborne Laser Scanning Data. *Remote Sens.* **2022**, *14*, 3480. [CrossRef]
27. Xu, D.; Wang, H.; Xu, W.; Luan, Z.; Xu, X. LiDAR Applications to Estimate Forest Biomass at Individual Tree Scale: Opportunities, Challenges and Future Perspectives. *Forests* **2021**, *12*, 550. [CrossRef]
28. Falkowski, M.J.; Smith, A.M.S.; Gessler, P.E.; Hudak, A.T.; Vierling, L.A.; Evans, J.S. The Influence of Conifer Forest Canopy Cover on the Accuracy of Two Individual Tree Measurement Algorithms Using Lidar Data. *Can. J. Remote Sens.* **2008**, *34*, S338–S350. [CrossRef]
29. Duncanson, L.I.; Cook, B.D.; Hurtt, G.C.; Dubayah, R.O. An Efficient, Multi-Layered Crown Delineation Algorithm for Mapping Individual Tree Structure across Multiple Ecosystems. *Remote Sens. Environ.* **2014**, *154*, 378–386. [CrossRef]
30. Goldbergs, G.; Maier, S.; Levick, S.; Edwards, A. Efficiency of Individual Tree Detection Approaches Based on Light-Weight and Low-Cost UAS Imagery in Australian Savannas. *Remote Sens.* **2018**, *10*, 161. [CrossRef]
31. Yu, X.; Hyyppä, J.; Vastaranta, M.; Holopainen, M.; Viitala, R. Predicting Individual Tree Attributes from Airborne Laser Point Clouds Based on the Random Forests Technique. *ISPRS J. Photogramm. Remote Sens.* **2011**, *66*, 28–37. [CrossRef]
32. Lupardus, R.C.; McIntosh, A.C.S.; Janz, A.; Farr, D. Succession after Reclamation: Identifying and Assessing Ecological Indicators of Forest Recovery on Reclaimed Oil and Natural Gas Well Pads. *Ecol. Indic.* **2019**, *106*, 105515. [CrossRef]
33. Du, L.; Pang, Y. Identifying Regenerated Saplings by Stratifying Forest Overstory Using Airborne LiDAR Data. *Plant Phenomics* **2024**, *6*, 0145. [CrossRef]
34. Watt, M.S.; Jayathunga, S.; Hartley, R.J.L.; Pearse, G.D.; Massam, P.D.; Cajes, D.; Steer, B.S.C.; Estarija, H.J.C. Use of a Consumer-Grade UAV Laser Scanner to Identify Trees and Estimate Key Tree Attributes across a Point Density Range. *Forests* **2024**, *15*, 899. [CrossRef]
35. Li, Y.; Xie, D.; Wang, Y.; Jin, S.; Zhou, K.; Zhang, Z.; Li, W.; Zhang, W.; Mu, X.; Yan, G. Individual Tree Segmentation of Airborne and UAV LiDAR Point Clouds Based on the Watershed and Optimized Connection Center Evolution Clustering. *Ecol. Evol.* **2023**, *13*, e10297. [CrossRef]
36. Hao, Y.; Widagdo, F.R.A.; Liu, X.; Liu, Y.; Dong, L.; Li, F. A Hierarchical Region-Merging Algorithm for 3-D Segmentation of Individual Trees Using UAV-LiDAR Point Clouds. *IEEE Trans. Geosci. Remote Sens.* **2022**, *60*, 1–16. [CrossRef]
37. Cao, L.; Coops, N.C.; Innes, J.L.; Sheppard, S.R.J.; Fu, L.; Ruan, H.; She, G. Estimation of Forest Biomass Dynamics in Subtropical Forests Using Multi-Temporal Airborne LiDAR Data. *Remote Sens. Environ.* **2016**, *178*, 158–171. [CrossRef]
38. Chen, X.; Jiang, K.; Zhu, Y.; Wang, X.; Yun, T. Individual Tree Crown Segmentation Directly from UAV-Borne LiDAR Data Using the PointNet of Deep Learning. *Forests* **2021**, *12*, 131. [CrossRef]
39. White, J.C.; Coops, N.C.; Wulder, M.A.; Vastaranta, M.; Hilker, T.; Tompalski, P. Remote Sensing Technologies for Enhancing Forest Inventories: A Review. *Can. J. Remote Sens.* **2016**, *42*, 619–641. [CrossRef]
40. Baah-Acheamfour, M.; Dewey, M.; Fraser, E.C.; Schreiber, S.G.; Schoonmaker, A. Assessing Ecological Recovery of Reclaimed Well Sites: A Case Study From Alberta, Canada. *Front. For. Glob. Change* **2022**, *5*, 849246. [CrossRef]
41. Brand, D.G.; Leckie, D.G.; Cloney, E.E. Forest Regeneration Surveys: Design, Data Collection, and Analysis. *For. Chron.* **1991**, *67*, 649–657. [CrossRef]
42. Goodbody, T.R.H.; Coops, N.C.; Queinnec, M.; White, J.C.; Tompalski, P.; Hudak, A.T.; Auty, D.; Valbuena, R.; LeBoeuf, A.; Sinclair, I.; et al. *sgsR*: A Structurally Guided Sampling Toolbox for LiDAR-Based Forest Inventories. *Forestry* **2023**, *96*, 411–424. [CrossRef]

Disclaimer/Publisher's Note: The statements, opinions and data contained in all publications are solely those of the individual author(s) and contributor(s) and not of MDPI and/or the editor(s). MDPI and/or the editor(s) disclaim responsibility for any injury to people or property resulting from any ideas, methods, instructions or products referred to in the content.